AMERICAN UNIVERSITY OF BEIRUT

SYNTHESIS, CHARACTERIZATION, AND PHOTOCATALYTIC PROPERTIES OF NEW HETERONANOSTRUCTURES BASED ON NIOBIUM OXIHYDROXIDES.

by
RAAFAT AMMAR ZIADE

A thesis
Submitted in partial fulfillment of the requirements
for the degree of Master of Science
to the Department of Chemistry
of the Faculty of Arts and Sciences
at the American University of Beirut

Beirut, Lebanon
February 2021

AMERICAN UNIVERSITY OF BEIRUT

SYNTHESIS, CHARACTERIZATION, AND PHOTOCATALYTIC PROPERTIES OF NEW HETERONANOSTRUCTURES BASED ON NIOBIUM OXIHYDROXIDES

by

RAAFAT AMMAR ZIADE

Approved by:

Dr Mohamad Hmadeh, Associate Professor Department of Chemistry	Advisor
Dr. Faraj Hasanayn, Professor Department of Chemistry	Member of Committee
Dr. Digambara Patra, Professor Department of Chemistry	Member of Committee

Date of thesis defense: February 24, 2021

AMERICAN UNIVERSITY OF BEIRUT

THESIS RELEASE FORM

Student Name: Ziade Raafat Ammar
Last First Middle

I authorize the American University of Beirut, to: (a) reproduce hard or electronic copies of my thesis; (b) include such copies in the archives and digital repositories of the University; and (c) make freely available such copies to third parties for research or educational purposes:

- ☐ As of the date of submission
- ☐ One year from the date of submission of my thesis.
- ☐ Two years from the date of submission of my thesis.
- ☒ Three years from the date of submission of my thesis.

Signature

Date
February 28, 2021

ACKNOWLEDGEMENTS

First and foremost, I would like to thank my thesis advisor, Dr. Mohamad Hmadeh for his continuous support during this journey. His mentor and guidance built my confidence in research and pushed me to become the future scientist I aspire to be, it was a long beautiful, and fruitful experience for me.

I would also like to express my sincere gratitude to my committee members, Dr. Faraj Hasanayn and Dr. Digambara Patra, for their constructive feedback and suggestions that supported my research and provided me with insights on how I can improve my work.

We are deeply indebted to the University of Toronto for the strong and sustained support of our solar fuels research. Dr. Mohamad Hmadeh and Dr. Benoit Mahler performed H_2 production reactions, HRTEM, and XPS at Ozin lab at the University of Toronto.

I would also like to extend heartfelt gratitude to the Central Research Science Laboratory (CRSL) staff for their support and training.

I would like to thank all of my colleagues in Dr. Hmadeh's group for their support and help during the long nights of doing research I will forever be indebted.

To Mahmoud and Salah, thank you for all the fun times we had together, and thank you for supporting me throughout this whole journey.

To my mother, father and sisters, no words can express my gratitude for your infinite support to go after my dreams. Your support was fundamental for me to be here today.

To my aunts, I am forever grateful for your support, the crazy overnights before the exams, and your infinite love.

To my soulmate Sarah, your unconditional love and support motivated me to withstand all the difficult times I had during this journey. I love you.

To my grandmother, may God bless her soul, you and my grandfather, may God give him health, were a second home for me here in Beirut. We had amazing memories; your never-ending love and care were beyond words. Her memory will be with me wherever I go.

ABSTRACT
OF THE THESIS OF

Raafat Ammar Ziade for Master of Science
Major: Chemistry

Title: Synthesis, Characterization, and Photocatalytic Properties of New Heteronanostructures Based on Niobium Oxihydroxides.

Heteronanostructured photocatalysts have attracted some good attention due to the enhanced catalytic activity of the multi-component material rather than its pure form. In this work, we successfully synthesized and characterized new Heteronanostructured samples of the semiconductor Nb_3O_7OH decorated with different metal loadings of Pt, Au, Cu, Pd, and Ag via a photodeposition technique. The compounds were characterized by XRD, UV-Vis absorbance, SEM, EDX, TEM, and Atomic absorption.

We first investigated the effect of Pt loading on catalytic H_2 production. The obtained results showed that the spillover mechanism is possible for low Pt loading which is responsible for the high production rate.

In the second part, we studied the photocatalytic degradation of Rhodamine B, and the best one of the tested compounds until now is the gold decorated compound with 0.5% as metal loading. Future work will include the exploration of the rest of the compounds and the effect of loading percentage will be studied regarding the effectiveness.

TABLE OF CONTENTS

ILLUSTRATIONS

Figure

TABLES

Table

CHAPTER I

LITERATURE REVIEW

A. The need for solar energy use: Semiconductors

These days, humanity largely depends on fossil fuels for producing energy (**Figure. 1**).[1] Unfortunately, this has caused a huge increase in the emission of CO_2 due to the combustion process and hence the need to explore other renewable energy resources is necessary. From the available energy resources, solar radiation seems the best option since it is relatively infinite. Actually, the solar radiation reaching the earth in one hour is more than enough to cover all the energy consumption needed for one year.[2]

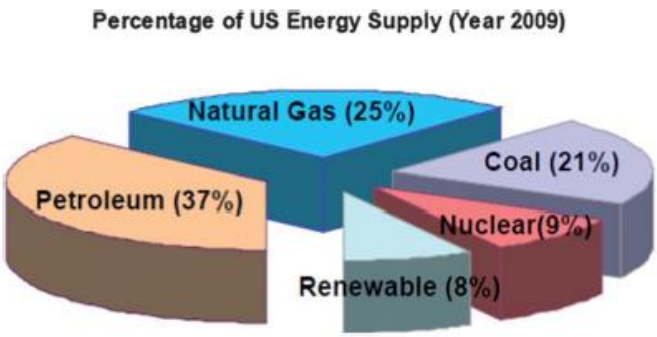

Figure 1 The diagram shows the percentage of the energy supplied from different sources in the US.[1]

Despite the fact that many methods are established to make use of the solar power such as concentrating solar power and solar photovoltaic technologies, the direct conversion of solar energy into chemical fuels, H_2 as a preference, is one of the best choices. Splitting water into H_2 and O_2 is the main objective since water is widely

available and the best source of hydrogen on earth and last but not least it is the product formed when H_2 fuel is burnt.[3]

Alternatively, due to the concerns regarding the emission of the greenhouse gas CO_2, methods to capture, store and utilize CO_2 is another urgent need. In particular, the transformation of CO_2 to fuels using catalysts drew a lot of attention in the past years.[4-6] Since the CO_2 molecule has a high stability, the photocatalytic conversion of CO_2 to useful fuel using solar power is the best path.

Fujishima and Honda were the pioneers in the photoelectrochemical splitting of water into H_2 and O_2 using TiO_2 electrodes under UV illumination in 1972.[7] In addition, Inoue *et al.* developed the photocatalytic reduction of CO_2 to organic molecules such as methanol, formaldehyde, and formic acid by irradiating CO_2 saturated aqueous suspensions with a Xe lamp and using several semiconductors like ZnO, SiC, WO_3, CdS, and TiO_2 in 1979.[8] Since these works, several studies have emerged in the past decades owing to the high demand for renewable energy and the environmental global concerns. Porous nanospheres, nanorods, nanotubes, nanowires were studied and proved to have suitable characteristics for the photocatalytic activity such as large surface areas, tunable light absorption, and low reflectivity. In addition, hybrid nanomaterials were synthesized, for instance, dye-sensitized nanoparticles, nanocrystals of semiconductor decorated with metallic clusters, quantum dots in nanowires, and core-shell nanowires all of which were proved to be photocatalysts with heightened efficiency.[9-12] In this regard, we will go over the essential challenges faced when designing semiconductors for use as photocatalysts and discuss the different methods used to improve their activities and their stability.

B. Essential challenges of semiconductor photocatalysts

The semiconductor is able to absorb the light irradiation (provided the energy of the photon is equal to or higher than the bandgap of the said material) and consequently converts the obtained energy into chemical energy. We can divide this process into four different steps (**Figure. 2**).[1] Step I is the photoexcitation, in this step, the photon will excite the negatively charged electrons in the valence band to the conduction band and create the holes, which have a positive charge forming what we call electron (e^-)-hole (h^+) pairs putting the catalyst in a photoexcited state. Step II is where charge separation and transportation take place, the electron hole pairs will split and migrate to their active sites on the surface of the photocatalyst or cocatalyst.

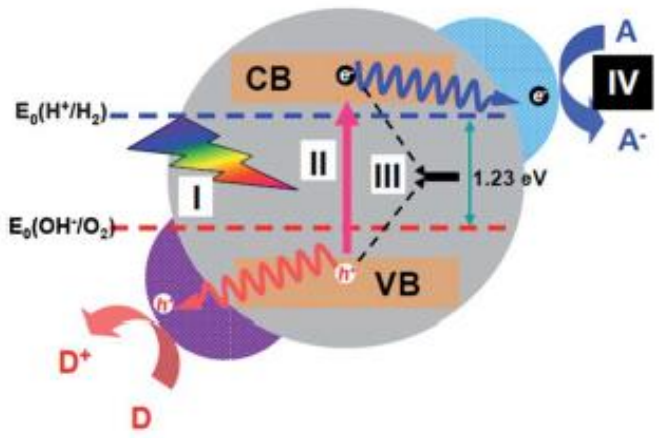

Figure 2 Schematic illustrating the mechanism for photocatalytic process on TiO_2 coupled with cocatalysts for redox reactions.1

At the same time, in step III, some of the photogenerated electrons and holes will recombine or be trapped by defects in the bulk material or the surface of the catalyst. Step IV comprises the reduction/oxidation reactions. The electrons and holes

will perform the reduction/oxidation reactions by acting as reducing and oxidizing agents respectively on the active sites of the photocatalyst/cocatalyst.

Photoassited splitting of water, photoreduction of CO_2, and light-driven degradation of organic pollutants are all important applications in the field of photocatalysis.

One problem is that many of the photocatalysts are limited in their activity due to the fact that they only function in the UV region since they have wide bandgaps like TiO_2. In addition, many of them have low efficiency due to incompetent charge separation and transport and/or photo corrosion of the semiconductor.[13] Here, we use the water-splitting reaction as a model to pinpoint the obstacles faced when designing a stable and efficient photocatalyst. Thermodynamically speaking, water splitting is a non-spontaneous reaction with a ΔG equal to 237.2 $kJ.mol^{-1}$ to break one water molecule to H_2 and ½ O_2 at standard temperature and 1 atm.[14] Practically speaking, the efficiency of solar water splitting depends on several aspects: (i) decreasing the path traveled by the photogenerated carriers to their respective sites on the photocatalyst surface;[15, 16] (ii) improving water adsorption by increasing the surface area of the catalyst;[17] (iii) facilitating charge separation by decreasing the feature size over the critical size[18] (iv) shifting the edges of the conduction band and/ or the valence band in order to improve the thermodynamic threshold of surface reactions.[19] In this case, the bandgap of the semiconductor for the solar-driven splitting of water should have the three following requirements: (i) the bandgap has to be higher than 1.23 eV to span the range of redox potentials for water splitting; (ii) the conduction band potential should be higher (more negative) than the water reduction potential; (iii) the valence band potential should be lower (more positive) than the water oxidation potential.[20, 21]

As mentioned earlier, TiO_2 only absorbs in the UV light with a bandgap of ~ 3.2 eV accounting only for 4% of the solar energy. However, other semiconductors can absorb in the visible region of the solar spectrum owing to their narrower bandgaps like CdS with a bandgap of ~ 2.4 eV.[3] We can see in **Figure. 3**[3] the band levels of many semiconductors along with the redox potentials of water oxidation and the reduction potentials of several species H_2 and CO_2. As stated previously, the reduction and oxidation potential should fall within the bandgap of the semiconductor for a successful overall photocatalytic reaction to occur.

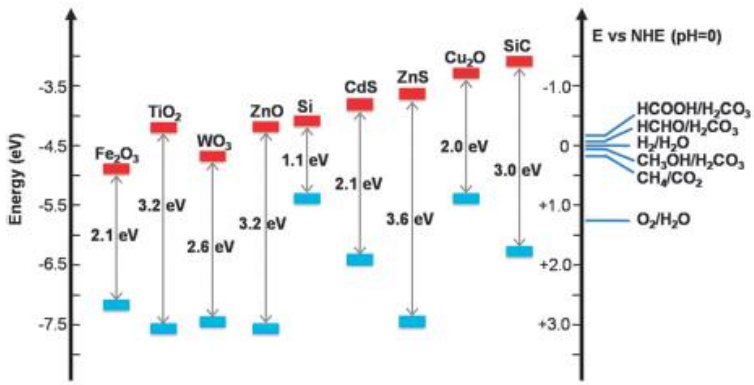

Figure 3 Bandgaps for different semiconductors relative to the redox potentials of several couples in water.[3]

C. Strategies to increase the efficiency of the semiconductor photocatalyst:

In the coming sections, we will highlight the previous achievements in the development of semiconductor photocatalysts and include the variant methods used to increase their efficiency. Those methods include: (i) fine-tuning of the bandgap in order to increase the absorption in the visible light portion of the solar spectrum and, at the same time, preserve the potential for the sought-after redox reactions; (ii) the use of

heterostructured semiconductors to increase the efficiency of charge separation and (iii) the use of a suitable cocatalyst to ease the overpotential of redox reactions

1. Efficient absorption of solar energy:

TiO_2 was very well studied as a photocatalyst for its efficiency, cheapness, and chemical durability. It was also proved that titania-based catalysts can be used efficiently in water splitting reactions.[22] Nevertheless, a major drawback in TiO_2 is its large bandgap (~ 3 eV). It can only absorb 5% of the solar irradiation, as UV or near-UV.[23] As a result, despite its effectiveness, TiO_2 and titania-based photocatalysts cannot be used for effective absorption of solar power and conversion. The real challenge is to develop photocatalysts that can absorb the visible light more effectively.

In this regard, major efforts were made to increase the efficiency of solar absorption of the semiconductor photocatalysts. All in all, three pathways were followed to enhance the visible light absorption: (1) doping of TiO_2, which includes the addition of metals or non-metals (like nickel, platinum, vanadium, chromium, tungsten, nitrogen, fluorine, sulfur, *etc.*);[7, 24, 25] (2) using other semiconductors with smaller bandgaps than that of TiO_2 (*e.g.*, Si,[26] InP,[27] CdSe,[28] and GaZnON;[29, 30] and (3) the incorporation of light sensitizers to increase the visible light absorption like organic dyes, metals or a semiconductor with a small bandgap).[31-34]

Lately, Chen *et al.* were able to improve the visible light absorption by making a disordered shell of numerous atomic layers of nanophase TiO_2 by means of a hydrogenation technique creating what was called “black TiO_2”.[35] This black TiO_2 had a higher efficiency in visible light photocatalysis in comparison to conventional white TiO_2. 0.2 $\pm$ 0.02 mmol of H_2 were produced using black TiO_2 decorated with 0.6% of Pt

by weight in a 1:1 water-MeOH mixture, this is about 100 times more than the production efficiency of the majority of the formerly reported semiconductor photocatalysts.[36] Afterwards, Y. Li and co-workers reached a 1.63% solar to hydrogen efficiency using the hydrogen treated TiO_2 nanowires which were used as a photoanode in the photoelectrochemical splitting of water.[37]

As for the substitutes of TiO_2, numerous novel photocatalysts have emerged; many of those semiconductors followed essentially two routes. The first one is finding native semiconductors with narrow bandgaps that can absorb in the visible region (*e.g.* α-Fe_2O_3, $BiVO_4$, Ag_3PO_4, and CdS), all of which are known as visible light photocatalysts.[38] The second route is the solid solutions of isostructural semiconductors.[36]

Domen's team investigated the GaN-ZnO solid solution system for photocatalysis[29, 30], which proved to split water into H_2 and O_2 under visible light illumination with the addition of redox cocatalysts.[39] The GaN-ZnO had a bandgap of 2.58 eV, which is smaller than the bandgaps of the individual semiconductors GaN and ZnO being 3.4 eV and 3.2 eV respectively. The narrowing of the bandgaps was explained according to DFT calculations: the p-d repulsion due to the presence of electrons in the Zn3d and N2p orbitals of the valence band results in shifting the valence band and subsequently narrowing the bandgap.[29] In a similar manner, several solid solutions (*e.g.*, CdS-ZnS, $AgInS_2$–$CuInS_2$, $CuInS_2$–$AgInS_2$–ZnS, $AgInS_2$–ZnS, and $CuInS_2$–ZnS) were investigated and showed to be active for photocatalytic H_2 production in aqueous sulfide and sulfite under visible light illumination.[36]

Narrow bandgap semiconductors, molecular dyes, and/or nanoscale metal particles are basically used in sensitizing agents on the photocatalyst surface to extend

the absorption to the visible region which will subsequently increase the overall catalytic efficiency. Numerous narrow bandgap semiconductors (*e.g.*, ZnSe,[40] PbS,[41] CdSe,[42, 43] InP,[44] and AgI,[45, 46], *etc.*) were used as sensitizers for semiconductors with large bandgaps like TiO_2, ZnS, ZnO, *etc.* for the visible light photocatalysis. On that basis, the narrow and the wide bandgap semiconductors have different electronic levels for their respective conduction band and valence band. Solely the narrow bandgap semiconductor is excited generating electrons in the valence band under visible light illumination. For the electrons to transfer from this sensitizer to the wide bandgap semiconductor, the level of the conduction band of the sensitizer should be higher than that of the semiconductor photocatalyst. Afterwards, the electrons generated in the sensitizer can transfer into the photocatalyst conduction band to do a reduction reaction. If the electronic level of the valence band of the photocatalyst is lower than that of the sensitizer, the photogenerated holes will stay in the sensitizer and perform the oxidation reaction (**Figure. 4**)[38].

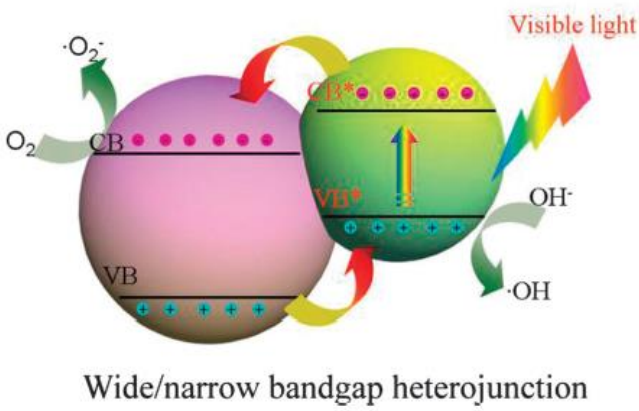

Figure 4 A scheme showing the transfer of photoinduced electron-hole pairs in a wide/narrow bandgap heterojunction under visible light illumination.[38]

From this scheme, several advantages are acquired: (1) the improved absorption of visible light; (2) a better charge separation; (3) an increase in the speed of charge injection into the photocatalyst; and (4) charge carries have a better lifetime. We can see in **Figure. 5** some of the explored narrow bandgap sensitizers for wide bandgap semiconductors.

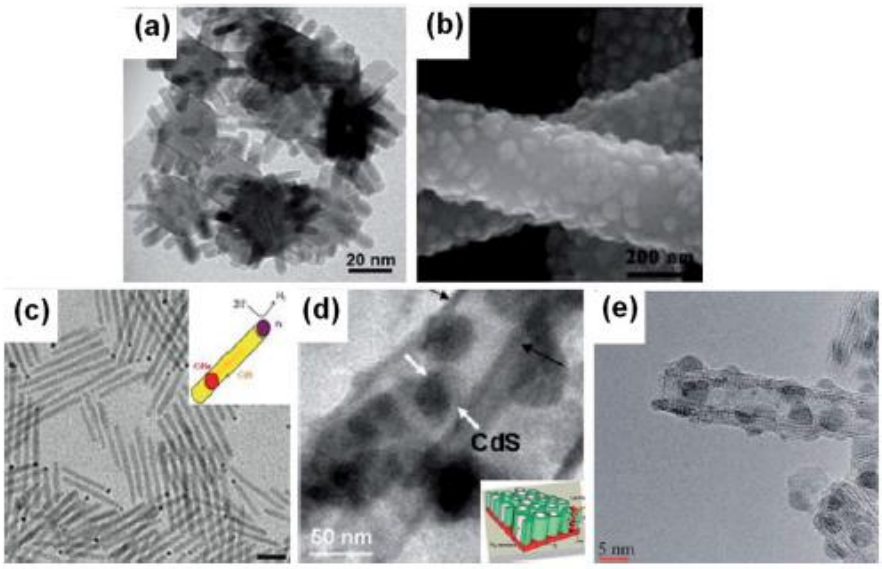

Figure 5 (a) $SnO_2/\alpha\text{-}Fe_2O_3$ (nanocube) under TEM.[47] (b) CeO_2/TiO_2 SEM image.[48] (c) Pt tipped CdS nanorod with embedded CdSe seed using TEM, inset shows an illustration of the heteronanostructure.[49] (d) TEM image of TiO_2 nanotubes with CdS nanoparticles filled inside, the inset shows an illustration of the structure.[50] (e) PbS/TiO_2 nanotubes under TEM.[51]

Molecular organic dyes were also used as sensitizers for wide bandgap semiconductors thanks to their absorption that falls in the visible light range.[52, 53] The dye sensitizers for light-driven catalytic reactions caught interest because of their well-known efficiency, cheapness, and stability.[54-56] In the dye sensitization procedure, the dye molecule absorbs light. After excitation, the electrons are injected from the dye to

the photocatalyst. An energy conversion efficiency of up to 11% was reached in dye sensitization.[56]

Organic dyes can be loaded on the wide bandgap photocatalysts or used without bonding (by means of electrostatic attraction to the surface of the catalyst instead) for the photocatalytic splitting of water or reduction of CO_2.[57] After the absorption of photons, the dyes will be in the electronic excitation state and the photoinduced electrons are transferred to the photocatalyst's conduction band. The electrons accepted by the photocatalyst can then proceed to perform the redox reactions. In the meantime, the oxidized dyes will be reduced and restored by accepting electrons from hole scavengers in the solution. The sacrificial agents usually used are I^{3-}/I^{-}, EDTA and triethanolamine. It essential to mention that the electron transfer from the dye to the photocatalyst is the critical step that dominates the solar conversion efficiency.[58]

Finally, another way to increase light-harvesting in the visible region is the use of metal nanoparticles and loading them on the surface of wide semiconductors like TiO_2. The effect brought about by the metals is called surface plasmon resonance and it is the reason for the increase in absorption efficiency.[59, 60]

Surface plasmon resonance (SPR) is the resonance energy that arises when the frequency of the coherent oscillation of conduction electrons that are on the surface volume of the metal nanoparticle coincides with the frequency of incident photons (**Figure. 6**).[13] The wavelength upon which the SPR effect is observed depends on several factors such as the metal used, shape, size, the surrounding dielectric environment, the distance that is between the objects in its vicinity, and the configuration of their structure. By changing those factors, many metallic nanostructures can be synthesized to make use of the fully visible solar spectrum.[61-65]

The special effect of those plasmonic metals in absorbing visible light, scattering light, and concentrating electric field makes them the perfect choice for photocatalysis,[66-68] biosensing,[69-71] photovoltaics,[72-74] and Raman spectroscopy.[75-77]

For many atoms like Sn, Pb, Cd, and In the SPR happens in UV region with little absorption band whereas noble metals like Au, Ag, and Cu have a strong plasmon resonance in the visible range. The tunability of those noble metals make them a perfect choice in the field of visible-light-driven photocatalysis.[78]

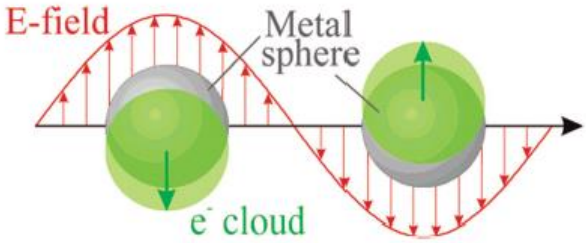

Figure 6 An illustration showing the displacement of the electron cloud relative to the nuclei in the plasmon resonance of a metal sphere.[13]

Many reported structures are using TiO_2-Ag and TiO_2-Au nanostructures for SPR enhanced photoactivity under visible light. They include and are not limited to: gold nanoparticles deposited on TiO_2 spheres,[79, 80] coatings on SiO_2,[81] nanotubes,[82, 83] nanoparticles,[84-93] film[94-96], photonic crystal,[97] layered titanate,[67] titanate nanoblets[98], and mesoporous titania[99, 100]. In a similar manner, numerous structures are reported for TiO_2-Ag nanocomposites.[101-108]

The mechanism by which the SPR effect improves the efficiency of the photocatalytic process is divided into three different classes:

- Electron transfer from the metal to TiO_2 induced by SPR:

This effect resembles very much the dye sensitization process in which the dye compound adsorbed to TiO_2 absorbs light and the photogenerated electrons are injected into the conduction band of TiO_2. In the case of plasmonic metals, the nanoparticles absorb resonant photons at the resonance frequency and the generated electrons that are SPR induced will be injected into the semiconductor (**Figure 7**)[109].[80, 86, 110-112]

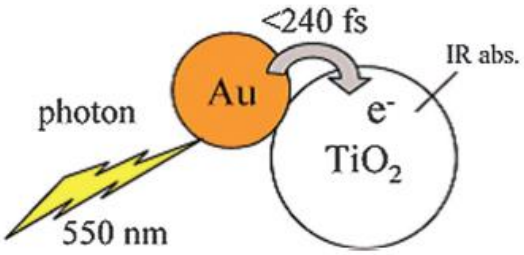

Figure 7 A diagram of a gold anchored to a TiO_2 nanoparticle with an indication of the electron transfer process.[109]

- The near-field electromagnetic enhancement:

  This is more pronounced when TiO_2 and the noble metal nanoparticle are separated by an insulator that blocks charge transfer between the two. The oscillation of electrons in the plasmonic metal is coupled with the electromagnetic field of incident photons and this results in an improvement in the localized electromagnetic field that is near to the surface of the plasmonic metal. The resulting enhancement is stronger than the field of photons that is needed to excite the nanostructure. The intensity of the field is the strongest at the surface and starts decreasing beneath it (around 20-30

nm).[94, 95, 103, 113] The induced electric field due to SPR can interact with TiO_2 when the semiconductor is close to the exciting plasmonic metal. It is this interaction that increases the rate of formation of excitons in local regions in the TiO_2 semiconductor because it is proportional to the local intensity of the electric field.[114-116]

- Scattering of photons mechanism:

  If the plasmonic nanostructures have a size larger than 50 nm, they will be able to scatter the resonant photons.[103, 117, 118] This scattering will increase the path traveled by photons in the TiO_2/metal structure (**Figure. 8**).[114] Therefore, the fact that photons are traveling longer paths will lead to an increase in the rate of formation of electron-hole pairs in the semiconductor.[103]

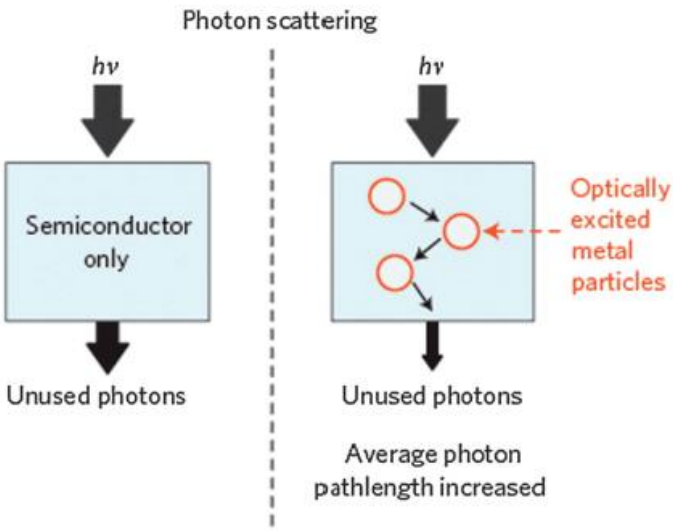

Figure 8 A scheme for the scattering mechanism. There is an increase in the path length of photons due to the presence of the plasmonic metal nanoparticles.[114]

Christopher *et al.*[117] proved the enhancement in methylene blue degradation thanks to the scattering mechanism of the photons from Ag to titania. In their study, cube-shaped Ag particles showed a better degradation efficiency of methylene blue than spherical Ag particles under UV illumination. The efficiency difference was explained by the fact that Ag cubes can scatter photons much more easily than Ag spheres.[117]

2. Photogenerated charge carriers' separation and transportation:

In this part, we discuss another important parameter for efficient photocatalysis: charge separation and transportation. Achieving efficient photocatalytic activity depends on the efficient separation of the generated electron-hole pairs and their rapid transfer to the adequate reaction sites. At the same time, charge recombination on the surface, of the photocatalyst, or on the way to it has to be decreased to the minimum.[119] Here we will show some strategies followed to achieve the aforementioned goals.

Noble metals and coinage metals such as Rh, Pd, Ru, Pt, Ag, Cu and Au are extensively used as cocatalysts in the hydrogen evolution and CO_2 reduction reactions.[120, 121]

Since the Fermi energy level of the metals is usually lower than that of the semiconductor, the photoinduced electrons can be trapped by the metal nanoparticles in the nanostructure. At the same time, the photoinduced holes will stay on the semiconductor. This is where the formation of the Schottky barrier takes place between the metal and the semiconductor and will eventually decrease the rate of electron-hole recombination.[122] We can see in **Figure. 9** the electrons flowing from the semiconductor to the metal since the latter has its Fermi level lying energetically below the conduction band of the semiconductor.[123, 124]

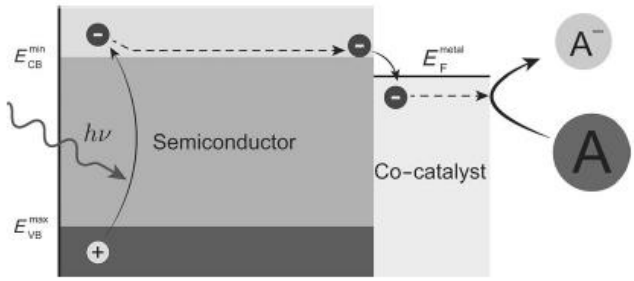

Figure 9 Photoinduced charge transfer from a semiconductor to the metal cocatalyst.[125]

Young *et al.* studied the efficiency of photocatalytic degradation of trichloroethylene and toluene by comparing two nanocomposites: TiO_2-Ag and TiO_2-Pt. The Pt decorated photocatalyst showed a better performance than the Ag decorated photocatalyst. The increased efficiency of TiO_2-Pt over TiO_2-Ag was explained by the difference in work functions of Ag and Pt. The work function of Ag (~4.26-4.29 eV) is smaller than that of Pt (~ 5.36-6.63 eV), the work function of TiO_2 is estimated to be 4.6-4.7 eV. Therefore, and according to the concept of Schottky barrier formation, the bigger difference in work functions between TiO_2 and Pt will lead to Pt being a better electron sink and will improve the electron-hole separation. Meanwhile, the smaller gap in work functions between TiO_2 and Ag is not sufficient for the charge separation.[126]

Another important strategy is the use of p-n heterojunction for its well-known efficient charge separation and transfer. In this scheme, the n-type and p-type semiconductors are in contact. Due to this contact, a space-charge region forms at the boundaries thanks to the diffusion of holes and electrons. As a consequence, an electrical potential is built that can drive the electrons and hole to transfer in opposite directions (**Figure. 10**). Upon light irradiation, the photoinduced electrons and holes are directly separated due to the built-in electric field of the space charge region. The electrons will be transferred from the semiconductor with the higher conduction band to

the second semiconductor with a lower conduction band. In the meantime, the holes will jump from the semiconductor with the lower valence band to the second semiconductor with the higher valence band. This way, charge separation and inhibition of charge recombination will be promoted more efficiently.[127]

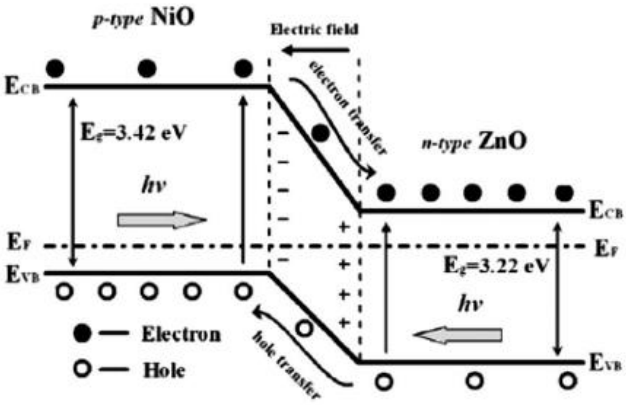

Figure 10 Diagram showing the Band structure and charge carrier separation in NiO(p-type)-ZnO(n-type) heterojunction.[127]

Hou *et al.* synthesized using an ion-exchange method with hydrothermal assistance a core-shell CdS@TaON heteronanostructure. The bandgaps of TaON and CdS are 2.5 and 2.45 eV, respectively. In this scheme, the photoinduced electrons are transferred from CdS to TaON owing to the higher conduction band of CdS. Meanwhile, the photogenerated holes jump from TaON to CdS. The CdS@TaON structure with 1wt% of CdS produced 306 μmol h^{-1} of H_2 when it was used for the photocatalytic H_2 evolution reaction in aqueous Na_2S and Na_2SO_3 solution under visible light illumination. Interestingly, when TaON and CdS were used alone for the same reaction, the produced H_2 amount was very low: 9 and 13.5 μmol h^{-1} for TaON and CdS respectively.[128]

An interesting type of semiconductor-semiconductor heterostructure is the Z-scheme. As mentioned earlier, for the complete water splitting reaction into hydrogen and oxygen, the conduction band of the photocatalyst should be more negative (higher) than the redox potential for H_2 evolution. By contrast, the valence band should be more positive (lower) than the redox potential for O_2 evolution. Nevertheless, not all semiconductors can satisfy both requirements and they can only proceed with one of the reactions due to mismatching of bands. This is where the Z-scheme is employed to overcome the issue by combining two semiconductors.[3] When using a Z-scheme framework (**Figure. 11**), the photoinduced electrons from the semiconductor having the higher conduction band will proceed to perform the reduction reaction (H_2 evolution in the case of water splitting). At the same time, the photoinduced holes from the semiconductor with the lower valence band will proceed to perform the oxidation reaction (O_2 evolution in the case of water splitting). Finally, the electrons generated in the semiconductor with the lower conduction band will recombine either directly or indirectly with the holes generated on the semiconductor with a higher valence band. The main feature of this scheme is the combined usage of a very strongly reductive electron from one semiconductor and the very strongly oxidative holes of the second.[3] In the case of indirect recombination of holes, reversible redox mediators like IO_3^-/I^- were used in several studies.[129, 130]

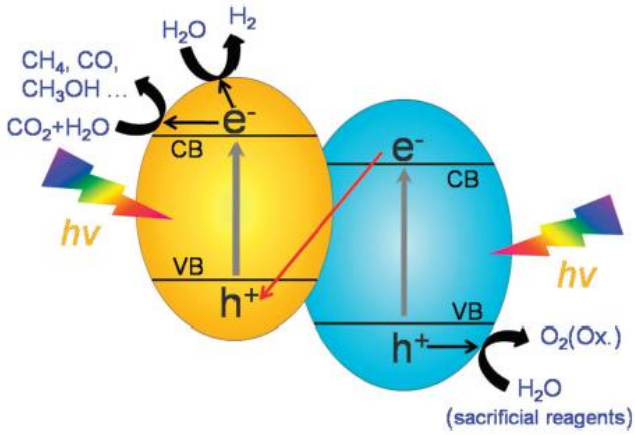

Figure 11 A scheme showing the charge transportation routes in the Z-scheme framework combining two semiconductors.[3]

Tada *et al.* synthesized a CdS-Au-TiO_2 composite where the Au nanoparticles had an average size of 3.4 nm and were deposited on the anatase TiO_2 whereas the CdS was coated on the Au nanoparticles owing to the good affinity of Au to S. The product formed, namely Au@CdS/TiO_2 (**Figure. 12**), was used under UV illumination. The photoinduced electrons transferred from TiO_2 to the gold nanoparticle and to CdS. The photoinduced electrons in CdS' conduction band perform the reduction reaction (H_2 evolution) whereas the photoinduced holes in TiO_2's valence band would perform the oxidation reaction. This scheme is not similar to the sensitization effect of TiO_2 using CdS since it was confirmed that the electron transfer from CdS to TiO_2 was minor. The added benefit of this scheme is restricting the photoinduced corrosion of CdS due to oxidation of S^{2-} on the surface by the photoinduced holes on CdS, since, the holes were combined with the photoinduced electrons from TiO_2 through Au.[131]

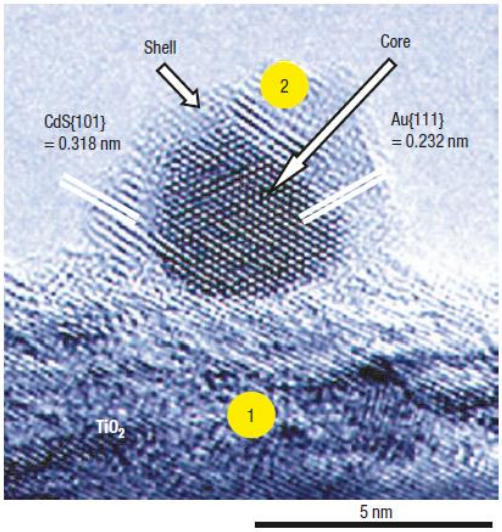

Figure 12 HRTEM of Au@CdS/TiO_2.[131]

Another used well-known material in enhancing the overall photoactivity of semiconductors is graphene. Graphene is a sp^2-hybridized carbons atoms two-dimensional structure. It has gained a lot of attention in the field of photocatalysis thanks to its amazing electrical properties like its good conductivity, efficient charge transfer capability, and large specific area (~2630 m^2g^{-1}). To date, many graphene/ semiconductor heterostructures have been investigated in the field of photocatalysis.[119] The observed improvement in the semiconductor-graphene heterojunctions can be explained by: (i) improvements in charge separation and transfer; (ii) increase of light absorption in the visible region and (iii) the good adsorption of reactants due to the high surface area.[38]

Several studies showed the increased benefit of having a semiconductor-graphene and a cocatalyst in the framework of photocatalysis. A TiO_2-MoS_2-graphene heterostructure was synthesized by Yu and co-workers in a two-step hydrothermal method and used for the UV-driven H_2 evolution reaction in an aqueous solution of ethanol. In the first step, MoS_2 nanosheets were dispersed on the graphene, and

afterward, in the second step, TiO_2 nanoparticles with an average size of 7 to 10 nm were formed on the MoS_2-graphene structure. The finished photocatalyst had a composition as per the following: 99.5% of TiO_2 and 0.5% MoS_2-graphene (made of 5% of graphene and 95% of MoS_2). The photocatalyst showed a higher H_2 evolution rate (165.3 μmol h^{-1}) than TiO_2-graphene (76.7 μmol h^{-1}) and TiO_2-MoS_2 (36.8 μmol h^{-1}) proving the synergistic effect of the ternary heterostructure. In this scheme, the photoinduced electrons in TiO_2 transfer from the conduction band to the graphene sheet whereby they can have efficient mobility reducing the rate of recombination with holes. Following this step, the MoS_2 dispersed on graphene will work as electron acceptors and thus as active sites for the H_2 production.[132]

3. *Addition of suitable cocatalysts for efficient redox reactions*:

Cocatalysts for redox reactions are an important aspect to consider in photocatalysis since they determine the fate of photoinduced charges used in the redox reactions. Because of the overpotential (activation energy), the photoinduced and separated charges may not be used efficiently in the redox reactions of interest without the use of specific cocatalysts to ease the overpotential. Several inorganic cocatalysts are used (*e.g.* Au, Pt, *etc.*) for the aforementioned issue.[129, 133]

Generally speaking, in the case of water splitting, cocatalysts can be divided into two groups: hydrogen production and oxygen production catalysts. The hydrogen production catalysts can be noble metals, such as Au, Pd, Pt, Ru, and Ag)[129]. Pt is actually one of the most effective catalysts for hydrogen evolution.[134] Also, some non-noble metals are also effective for hydrogen evolution such as MoS_2.[135] Other important catalyst include first-row transition metals, such as Co and Ni, complexes.[136, 137] On the

other hand, oxygen production catalyst include transition metal oxides of Ru, Ir, Mn, Co. Complexes containing those metals proved effective for the oxygen evolution activity.[138, 139]

Domen and co-workers studied the photocatalytic water splitting reaction over the GaN:ZnO photocatalyst and loaded it with Mn_3O_4 nanoparticles for O_2 evolution and Rh/Cr_2O_3 (core/shell) nanoparticles for H_2 evolution. The bi-cocatalyst system showed successful production of both H_2 and O_2 under visible light. It was proposed that the Cr_2O_3 shell quenched the backward reaction, that is H_2O formation, which would easily proceed on bare Rh sites. This happens because O_2 cannot penetrate the Cr_2O_3 shell and only H_2 can. On the other hand, the addition of Mn_3O_4 nanoparticles worked as efficient O_2 evolution cocatalysts.[39, 140]

D. Niobium based materials as promising photocatalysts:

In addition to the different forms of photocatalysts mentioned before, it is important to mention out niobium-based materials which are known for their non-toxicity and chemical stability with regard to light irradiation.[141] Niobium-based materials, were investigated in the field of photocatalysis thanks to their morphological and electronic properties that are suitable for light-driven catalysis. Nb is characterized by its well-known affinity to oxygen, and, niobium oxides show different properties based on the method of preparation and the target application.[142, 143] Niobium pentoxide is known to be one of the thermodynamically stable Nb-based materials. Having many different configurations, this compound can have bandgap energy varying between 3.2 eV to more than 5 eV.[144, 145]

Other than Nb_2O_5, Nb can form with oxygen extended lamellar compounds having polyoxy anions. These niobates are formed of negatively layered stacks intercalated with cations.[146] This kind of arrangement gives a high surface area and a good level of post-modification, superficial post-modification, or synthesis of nanoscrolls and nanosheets.[147-149] Also, Nb can be used as a good doping agent for changing the matrix crystalline structure and decrease the recombination rate of photoinduced charges.[150-153]

Bulk Nb_2O_5 by itself does not have a good photocatalytic activity due to the low specific surface area and because of the high rate of recombination for the photoinduced electron-hole pairs.[154] However, several studies managed to increase the efficiency by manipulating the morphology and shape of the particles in order to change Nb_2O_5's properties. Wen and coauthors successfully synthesized orthorhombic Nb_2O_5, named O-Nb_2O_5, by means of the hydrothermal method. They used $K_4Nb_6O_{17}4.5H_2O$ as a precursor. The finished product was constituted of rectangular nanosheets with a dominance exposure of the (010) facet (**Figure. 13**a-d). The obtained product was actually synthesized via an ion-exchange method by treating the precursor with acid and then the material was hydrothermally treated for 24 h at varying pH (1.5-11.5) and temperature conditions (195-215°C) (**Figure. 13**e). First, at a pH of 3.5 and with temperature changing, the XRD (X-ray diffraction) data displayed that O-Nb_2O_5 started forming at 200°C, and that at 210°C, $H_4Nb_6O_{17}3H_2O$ peaks fully vanished and that all displayed peaks were attributed to O-Nb_2O_5. From **Figure. 13**e, it is shown that in all pH values the O-Nb_2O_5 was successfully obtained but at pH=3.5 the formed material showed the highest crystallinity and more consistent morphology. For comparison, commercially available O-Nb_2O_5 was used and it had a spherical morphology and a

bandgap value of 3.2 eV, whereas the synthesized O-Nb_2O_5 had a value of 3 eV. The photoelectrochemical performance for both samples was studied using photocurrent measurements from the H_2 evolution reaction under UV illumination at 370 nm. Under illumination, the rectangular O-Nb_2O_5 nanosheets showed 4.3 times higher photocurrent value than that of the commercial O-Nb_2O_5. The better photoactivity was ascribed to the following: (i) larger amount of photoinduced charge carriers owing to the exposed (010) plane of the nanostructure with lower bandgap energy; (ii) less recombination sites and (iii) fast charge transport due to the high crystallinity of the rectangular nanosheets.[155]

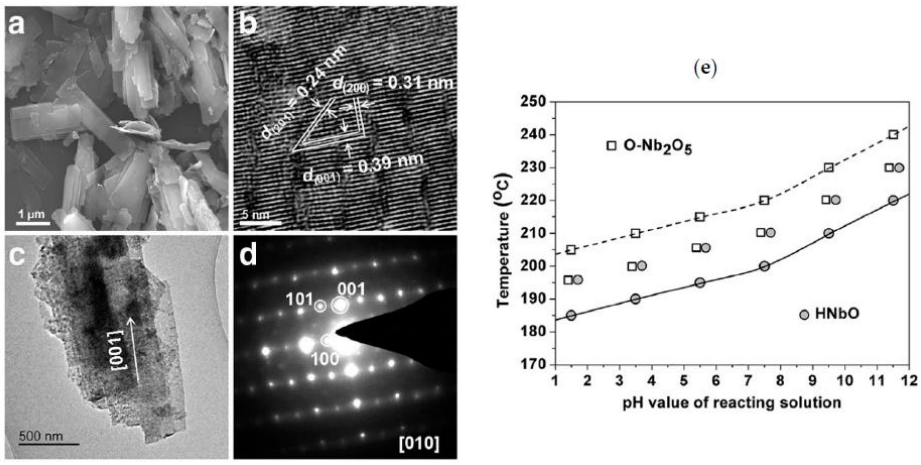

Figure 13 (a) FE-SEM image of O-Nb_2O_5, (b) HRTEM of O-Nb_2O_5, (c) TEM of O-Nb_2O_5, (d) SAED pattern, and (e) diagram showing the different hydrothermal conditions used to obtain O-Nb_2O_5 from $H_4Nb_6O_{17}3H_2O$ (HNbO).[155]

Concerning layered niobates, they are compounds formed of repeating octahedral NbO_6 units linked by opposite or adjacent sharing of corners or edges. This assembly results in a 2D extended layered arrangement. The configuration is made by stacked negatively charged layers with intercalation of cations.[146, 156]

One of the well-known and studied layered niobates is HNb_3O_8. Actually, the use of HNb_3O_8 was previously reported in several photocatalytic reactions: oxidation of amines,[157] oxidation of benzylic alcohols,[158] usages as the photo-anode in dye-sensitized solar cells,[159] CO_2 reductions to methane[160], and the hydrogen evolution reaction[161].

Very recently, HNb_3O_8 was used to produce a stable heteronanostructure photocatalyst. Xia and coauthors investigated a method to grow NiS with homogenous dispersion on the surface of HNb_3O_8. Generally, NiS particles use in light-induced H_2 production is problematic since they easily agglomerate and do not disperse easily in a homogenous way on the surface of the photocatalyst. In their study, the authors managed to deposit NiS on the HNb_3O_8 sheets using a self-assembly/ electrostatic adsorption method. The light-driven H_2 evolution reaction was examined using a 300 W Xenon lamp in an aqueous solution of triethanolamine (10%) where they used bare NiS and KNb_3O_8 produced negligible amounts of H_2. Using the prepared composite of 1 wt% NiS on HNb_3O_8 nanosheets in the same photocatalytic conditions led to the production of 1519.4 μmol $g^{-1}h^{-1}$ of H_2 which was higher than the amount produced by the physical mixture of both components (582.5 μmol $g^{-1}h^{-1}$). Time-resolved fluorescence decay data were used to estimate the lifetime of the photoinduced charge carriers. It was found from the kinetic data that the decay of the composite was slower, this indicated that the method used in the synthesis of the photocatalyst resulted in an efficient consumption of photoinduced charge carriers.[162]

Nb_3O_7OH nanorods were synthesized using a hydrothermal method. Then, CuO and Pt nanoparticles were deposited on the surface of Nb_3O_7OH using a microwave-assisted method. The finished products, Pt-Nb_3O_7OH and CuO-Nb_3O_7OH had uniform particle dispersion (**Figure. 14**). Both photocatalysts were used in the solar light-driven

H_2 evolution reaction. Pt-Nb_3O_7OH produced 710.4 μmol $g^{-1}h^{-1}$ of H_2 with a quantum efficiency of 5.40% at a wavelength of 380 nm. Regarding the CuO-Nb_3O_7OH compound, the authors found that it was inactive under solar illumination during a starting phase in which the heteronanostructure is photo reduced *in-situ* producing the active form which is Cu-Nb_3O_7OH. The solar-driven H_2 evolution reaction was studied for this compound and the H_2 production rate was estimated to be 290.3 μmol $g^{-1}h^{-1}$

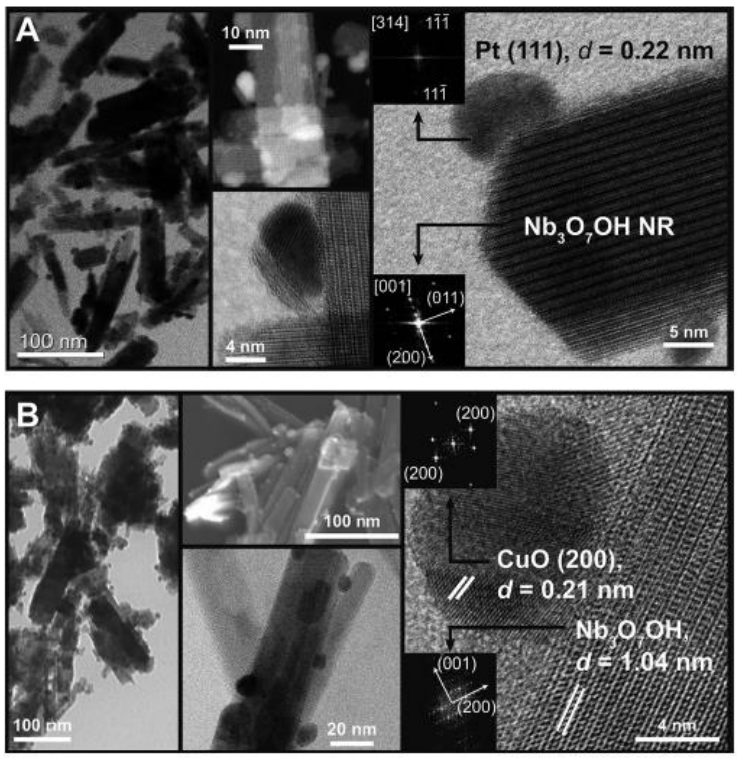

Figure 14 HRTEM images and FFT calculations of (A) Pt-Nb_3O_7OH and (B) CuO-Nb_3O_7OH.[161]

E. Objectives

In this research project, we first investigated the effect of Pt nanoparticles (Nps) size on Hydrogen production. The Pt Nps were deposited on the surface of Nb_3O_7OH by photodeposition. **Figure. 15** shows the crystal structure of Nb_3O_7OH. In this study,

we are interested in knowing the underlying mechanism for the production of H_2 on the surface of the photocatalyst. In particular, we wanted to know the correlation between the Pt size deposited on Nb_3O_7OH with respect to the change in H_2 formation rate. With the aid of the XPS technique, we can see what is happening on the surface and hopefully reach for a proposed mechanism of the photocatalytic reaction.

In a second part, we decorated Nb_3O_7OH by Cu, Pd, Au, and Ag via the same photodeposition process and we investigated their photocatalytic properties for the degradation of Rhodamine B (**Figure. 16**). Since as proposed earlier, the mentioned decoration metals can serve as aids in the photogeneration of electrons and holes due to the SPR effect. In this study, new photocatalysts are synthesized and will be used in the degradation of the toxic dye Rhodamine B that can cause many health and environmental concerns.

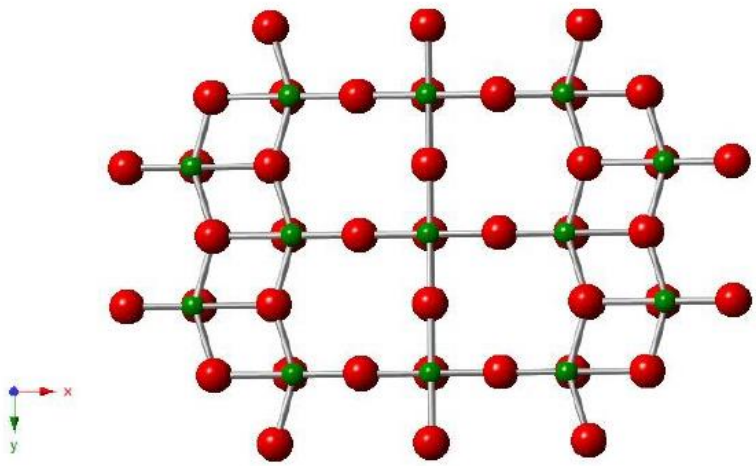

Figure 15 Crystal structure of $Nb_3O_7(OH)$; niobium in green, oxygen in red, hydrogen not shown.[161]

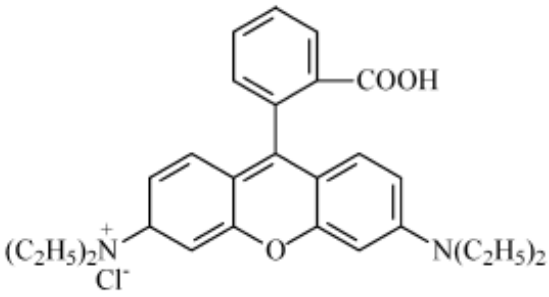

Rhodamine B (RhB)

Figure 16 Molecular structure of Rhodamine B.[163]

CHAPTER II

EXPERIMENTAL SECTION

A. Project I:

1. Materials synthesis:

Nb_3O_7OH nanorods: $Nb_3O_7(OH)$ nanorods were synthesized according to the reported procedure.[161] Typically, 0.2 g of Nb(s) were dissolved in 10 ml of HCl (8M). After sonication, the mixture was put in a Teflon-lined stainless steel autoclave at T=200 °C for 12 h, After cooling the product was washed three times with water and then vacuum dried at T=70 °C for 5 h (Figure. 17).

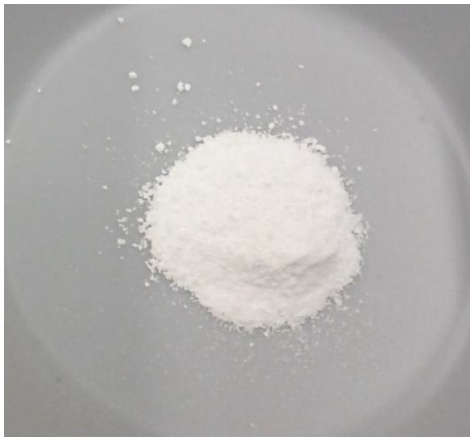

Figure 17 Nb_3O_7OH sample collected after hydrothermal synthesis

Platinum photodeposition: In a 250 mL two-neck flask, 50 mg of $Nb_3O_7(OH)$ nanorods are introduced along with 180 mL of a 1:1 H_2O/EtOH volume mixture and sonicated for 30 min. The dispersion is then illuminated for 3 h using a UV-finger under

magnetic stirring. The dispersion turns slightly blue at this point, indicating the accumulation of photogenerated electrons into the $Nb_3O_7(OH)$ rods. A solution of H_2PtCl_6 in EtOH (0.5M in Pt) is then swiftly injected, inducing an immediate color change from blue back to white. The dispersion is then illuminated with UV light for one more hour to ensure that all the Pt species are consumed. If the Pt concentration is high enough, the dispersion turns gray after this step. The resulting Pt–$Nb_3O_7(OH)$ nanorods are precipitated by centrifugation and washed twice by repeated re-dispersion in ethanol and centrifugation.

2. Characterization techniques:

TEM: Transmission electron microscopy (TEM) images were acquired using a TEM JEOL 2010F operating at 200 keV.

PXRD**:** Powder X-ray diffraction (PXRD) patterns were recorded on a Bruker D2 Phaser diffractometer (Cu Kα radiation).

XPS: X-ray photoelectron spectroscopy was performed at the University of Toronto inside an ultrahigh vacuum chamber with a base pressure of 10^{-9} Torr. The system is a Perkin Elmer Phi 5500 ESCA spectrometer operating with an Al Kα source. The high-resolution XPS spectra were obtained with an analyzer pass energy of 23.5 eV. The samples used for XPS analysis were prepared by spin coating the Pt–$Nb_3O_7(OH)$ dispersions on p-doped Si(100). All data analyses were carried out using the Multipak fitting program. The binding energies were referenced to the NIST-XPS database.

3. Photoactivity testing:

All photocatalytic tests were performed in a home-built, gas-tight quartz reactor developed by Dr. Hmadeh and Dr. Veronica Hoepfner at Ozin lab at the University of Toronto. The photocatalyst powder (200mg•L^{-1}) was dispersed in distilled water and methanol (25 vol%, HPLC grade). Before each run, the reactor was purged with nitrogen for 20 min and a background reference sample was taken as control. A Newport 300 W Xe lamp was used for solar irradiation and an air mass (AM) 1.5 filter (Newport) was applied to simulate the direct solar spectrum when the sun is at a zenith angle of 48.2°. Gas samples were extracted with a gas-tight syringe, separated by gas chromatography (GC, Agilent 7820A GC), and detected by a thermal conductivity detector (TCD). A 1.5m Molesieve 13X column (80–100 mesh) was used for the separation of H_2, O_2, and N_2, while an integrated 1m Haysep Q column (80–100 mesh) separates CO_2 and water vapor to avoid the contamination of the Molesieve column.

B. Project II:

1. Materials synthesis:

Metal photodeposition: All subsequent decorated products were synthesized following a photo deposition method, 100 mg of Nb_3O_7OH were sonicated in 220 ml of ethanol, this was followed by the addition of the metal-based salt of the needed decoration metal ($CuCl_2$, $H_2N_2O_7Pd$, $HAuCl_4.3H_2O$ or $AgNO_3$). After further sonication, the UV- finger was inserted and the reaction was run overnight under stirring. The as-synthesized product was centrifuged, washed 3 times with deionized water, and then dried under vacuum overnight at T=70 °C.

Two different metal loadings products (0.5% and 0.1% by weight) were synthesized for each metal (Au, Pd, Cu, and Ag). The exact loading percentage was calculated based on the weight of Nb_3O_7OH using atomic absorption (AA).

2. Characterization techniques:

XRD: Powder X-ray diffraction (PXRD) patterns were collected using a Bruker D8 advance X-ray diffractometer (Bruker AXS GmbH, Karlsruhe, Germany) at 40 kV, 40 mA (1600 W) using Cu-Kα radiation (λ = 1.5418 Å). The PXRD patterns were collected via 2θ from 20˚to 60˚and a step size of 0.01˚overnight.

UV-Vis: The absorption spectra were recorded at room temperature using JASCOV-570 UV-vis-NIR spectrophotometer. The samples were collected and UV-Vis measurement was performed.

SEM and EDX: Scanning electron microscopy (SEM) was performed using a MIRA3 Tescan electron microscope, where the samples were first coated with a thin layer of platinum at an acceleration voltage of 5-15 kV.

Atomic Absorption: Measurements were done using a THERMO SCIENTIFIC, ICE 3000 SERIES Atomic Absorption Spectrometer. Samples were dissolved in 1 ml aqua regia and diluted with deionized water before each measurement.

3. Photoactivity testing:

The photocatalytic degradation experiments were done on aqueous Rhodamine B solutions. Typically, 125 mg of the catalyst was dispersed in a 50 ml Rhodamine B solution (10 ppm). The photoreactor was equipped with a 100 w xenon lamp, a magnetic stirrer, and a jacketed beaker to maintain a constant temperature (Figure. 26).

Prior to irradiation, the mixture was stirred in dark for 50 min to attain the adsorption equilibrium. Samples were taken at time intervals and the residual Rhodamine absorption was detected by a spectrophotometer **(Figure. 18**). As a control experiment, a solution of Rhodamine B (10 ppm) without the catalyst was irradiated with light with no decrease in the concentration of residual Rhodamine B over 3 hours.

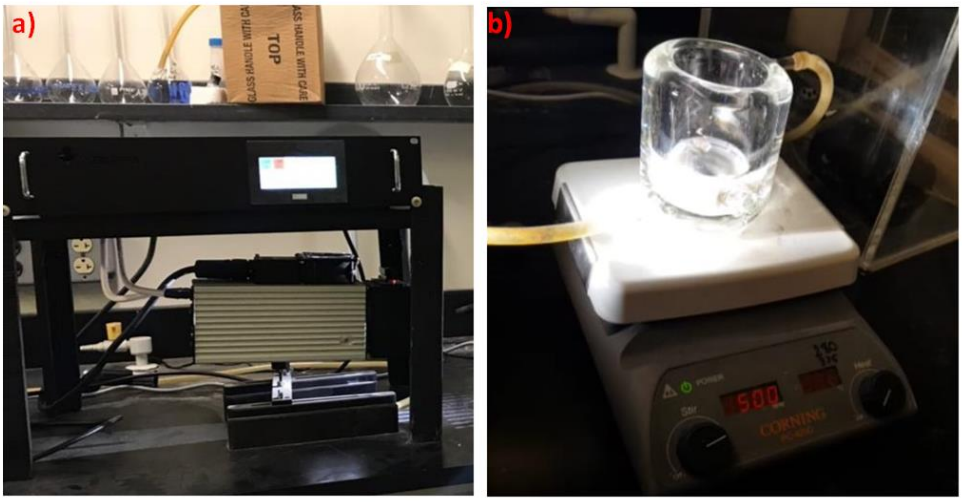

Figure 18 Photographic images of (a) Home built reactor and (b) Photoactivity run showing the jacketed beaker used.

CHAPTER III

SIZE EFFECT OF PLATINUM NANOPARTICLES PHOTO-DEPOSITED ON NB_3O_7OH NANORODS

A. Results and Discussion

Triniobium hydroxide heptaoxide, $Nb_3O_7(OH)$ is a wide band-gap semiconductor (about 3.85 eV). It has been recently reported as an efficient electrode for dye-sensitized solar cells[159] and photocatalyst for hydrogen evolution when it is decorated with metallic nanoparticles (platinum or copper). The valence and conduction band positions of $Nb_3O_7(OH)$ straddle the water oxidation and reduction potentials,[161] making it a potential photocatalyst for water splitting. Furthermore, the location of its conduction band suggests it can a promising photocatalyst for CO_2 reduction.

Contrarily to other semiconductors such as TiO_2, the pristine nanoparticulate $Nb_3O_7(OH)$ does not exhibit any photoactivity in hydrogen evolution conditions (i.e. light illumination in presence of a hole scavenger such as methanol). The semiconductor turns blue during light exposure, indicating the generation and accumulation of conduction band electrons and would return to its initial white color when exposed to air.[161]

SEM and TEM imaging of the obtained powder showed homogeneous nanorods of around 100 nm (**Figure. 19**). The PXRD patterns **(Figure 20)** clearly show that the experimental peaks of the decorated compounds are in agreement with the peaks of the pure non-decorated Nb_3O_7OH. This proves that the decoration did not affect the crystallinity of the Nb_3O_7OH semiconductor. Moreover, no additional peaks for the

metal loaded were observed due to the low loading percentage. Finally, the poor quality of the pattern reflects the small particle size of the nanorods of Nb_3O_7OH.

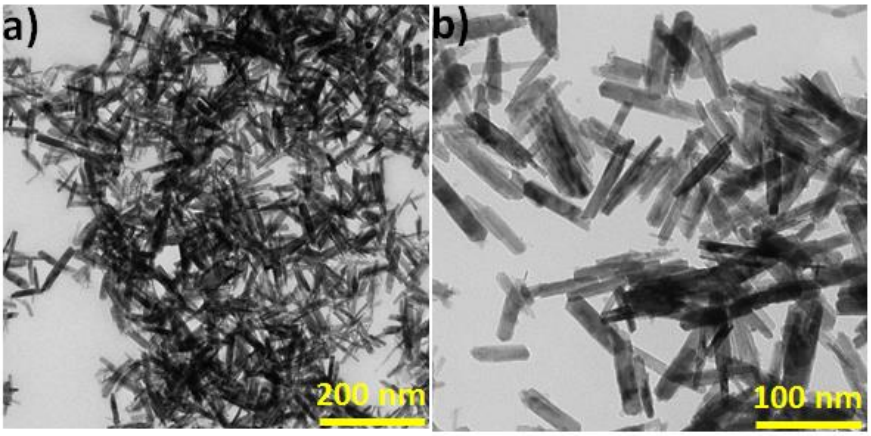

Figure 19 TEM images (a) and (b) of Nb_3O_7OH showing Nanorods of around 100 nm size

Surprisingly, it is possible to detect stable composition changes after illumination. X-ray photoelectron spectroscopy (**Figure. 20**a) reveals a drastic change in the oxide/hydroxide ratio, going from 8 (in good agreement with a theoretical value of 7) for the pristine $Nb_3O_7(OH)$ nanorod sample to 2.2 for the illuminated sample. Such a strong hydroxide increase does not induce any structural changes, as shown by the powder X-ray diffractogram of the sample before and after illumination (**Figure 20**b). There is no visible shift in any of the peaks and hence no distortion in the structure. A plausible mechanism to account for this hydroxide increase would be the photoreduction of the niobate compound when the holes are scavenged by the methanol:

$$Nb_3O_7(OH) + e^- + H^+ \rightarrow Nb_3O_6(OH)_2,$$

$$CH_3OH + 2\ h^+ \rightarrow CH_2O + 2\ H^+.$$

The generated hydroxides could either sit on the nanoparticle's surface or the generated protons can diffuse into the nanostructure itself. This increase in hydroxide content does not modify the valence band or the work function measured by XPS and the nanoparticles are still able to photo-reduce metals like gold or platinum.

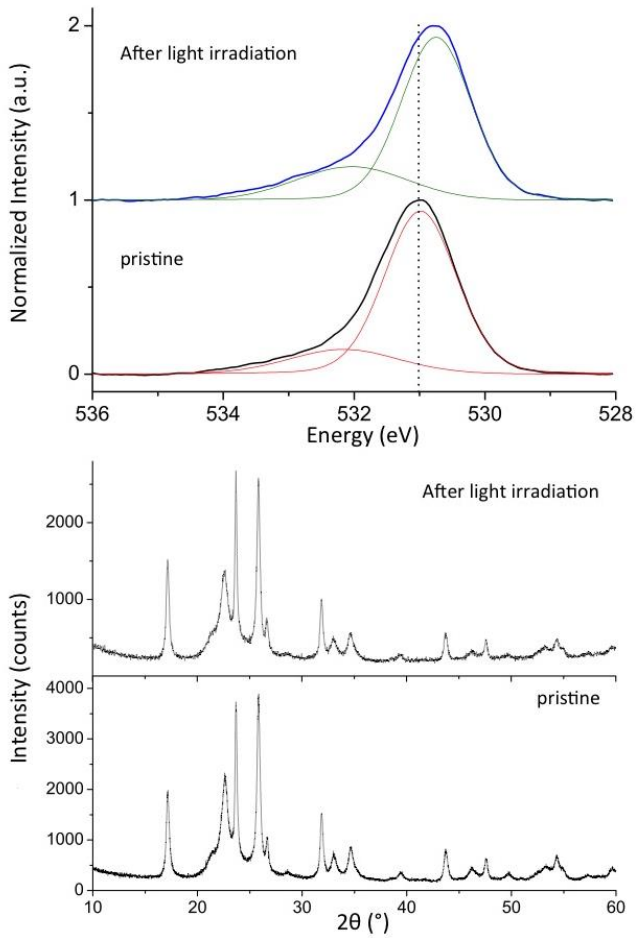

Figure 20 (a) X-ray photoelectron spectroscopy spectra of $Nb_3O_7(OH)$ before (black) and after (blue) illumination. (b) Powder X-ray diffractograms of $Nb_3O_7(OH)$ before (black) and after (red) illumination.

A protocol is developed to study the photodeposition of platinum on the hydroxide-rich $Nb_3O_7(OH)$ nanorods. Dispersion of nanoparticles in a water/ethanol

mixture is photo-irradiated to induce a hydroxide increase. Different amounts of platinum precursors (chloroplatinic acid) are then injected into the dispersion, which is illuminated for one more hour to ensure the complete reduction of the metal salt. Characteristic TEM images of $Nb_3O_7(OH)$ nanorod samples with different Pt loading and the histograms of their size distributions are presented in **Figure. 21**. A few conclusions can be drawn from this set of experiments. First, the hydroxide increase in the niobate nanorods does not lead to suppression of the photoactivity, and platinum photodeposition is still efficient. As expected, the mean size of the platinum nanocrystals can be adjusted by the amount of Pt precursor injected. The Pt nanocrystals size distribution is narrow, as evidenced in figure 2d. Surprisingly, the high Pt-loading samples have multiple Pt nanocrystals on the surface of the niobate nanorods. This shows that the photodeposition method does not prevent the formation of multiple nucleation sites (**Figure. 21** b,c). The platinum deposition on the $Nb_3O_7(OH)$ nanorods make them efficient photocatalysts for hydrogen evolution in the presence of a hole scavenger such as methanol. As previously reported on other systems, the hydrogen formation rate is strongly dependent on the platinum loading (**Figure. 22**, red curve) and reaches a maximum rate of 1.77 mmol g^{-1} h^{-1} at 0.2 weight % Pt loading. The hydroxide content of the niobate system is strongly dependent on the platinum loading (**Figure. 22**, black curve). At low platinum loading, the hydroxide content stays high, with an oxide/hydroxide ratio around 2.2, which is the value for the $Nb_3O_7(OH)$ nanorod sample after illumination. On the other hand, at high platinum loading, the oxide/hydroxide ratio has a similar value to the pristine $Nb_3O_7(OH)$ nanorod value around 8. It is interesting to note that the highest hydrogen evolution activity is reached when the hydroxide content is high.

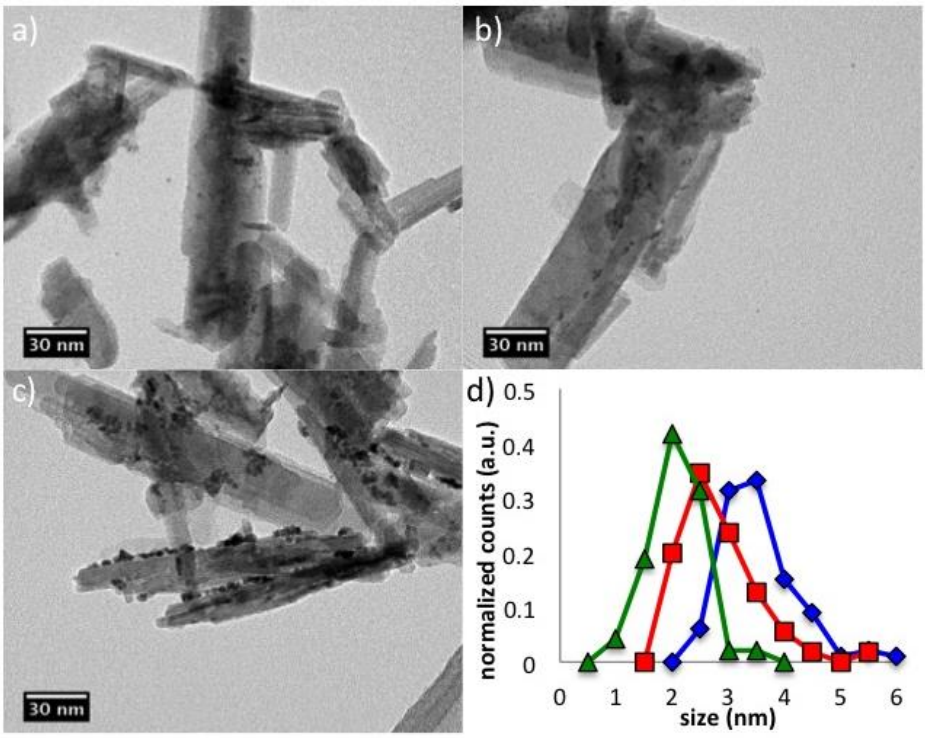

Figure 21 Low magnification TEM images of $Nb_3O_7(OH)$ nanorods after photodeposition of different amounts of platinum: (a) 0.3 weight %, (b) 1 wt % and (c) 4 wt %. (d) Normalized size distribution histograms of the Pt nanoparticles for the 3 platinum loadings: 0.3

A hypothesis would be a combination of the two mechanisms: reverse hydrogen spillover at low Pt loading and electron charge transfer[164] at high ones. In this case, low platinum loading will maintain a high photogenerated hydroxide content whereas the electron charge transfer and proton reduction processes occurring at the surface of the bigger Pt nanoparticles will prevent hydroxide accumulation in the system. Furthermore, the charge transfer mechanism decreases at the same rate as the number of active sites (localized solely on the platinum), which in turn decreases the hydrogen generation rates. The transition between the two mechanisms is then governed by the mean size of the Pt nanocrystals. Small Pt clusters possess few discrete electronic levels

separated in energy, which strongly decreases the probability of electron transfer to the metal. On the other hand, larger nanocrystals possess a lower work function and a higher density of states, facilitating a fast electron transfer from the semiconductor to the metal (**Figure. 23**).

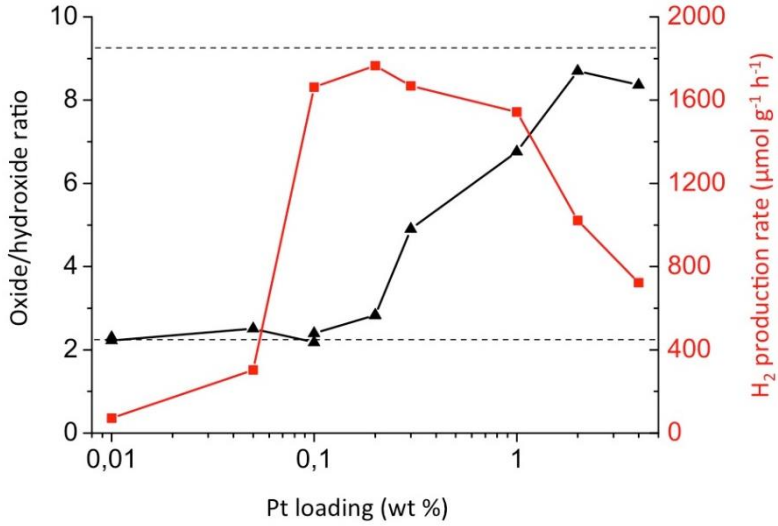

Figure 22 Photocatalytic hydrogen production rates as a function of platinum loading (red) and oxide/hydroxide ratio as measured by XPS (black).

In this table, we compared our photocatalyst to some reported[165-169] Pt decorated photocatalysts:

Photocatalyst	**Light source**	**H_2 formation rate/µmol g-1 h-1**	**Ref**
Pt/TiO_2	100 W UV Hg	3300	165
Pt/CdS	500 W Hg	153.8	166
$Pt/AgIn_5S_8$	400 W Xe	200	167
Pt/CdS:Ag	900 W Xe	28600	168
$Pt/AgInZn_7S_9$	300 W Xe	3133	169
$Pt\text{-}Nb_3O_7OH$	300 w Xe	1700	This work

Table 1 A comparison between our catalyst and some of the reported Pt decorated catalysts for H_2 production.

This shows that the activity of our photocatalyst in the same order of magnitude as some previously reported Pt decorated photocatalyst.

In the first study, $Nb_3O_7(OH)$ nanorods decorated with different platinum loading, were investigated for hydrogen evolution reactions. The hydroxide content correlates with the photoactivity and can be tuned by the amount of platinum deposited on the nanorods. The observed behavior can be well explained considering two competitive reaction mechanisms: a reverse hydrogen spillover[164] mechanism taking place at low platinum loading and a charge transfer mechanism occurring at high platinum concentrations(**Figure. 24**). The highest photocatalytic hydrogen evolution rates are observed when the reverse hydrogen spillover mechanism takes place: at low platinum loading, between 0.1 and 1 weight %.

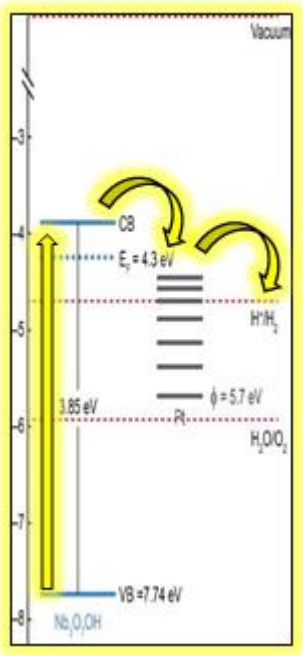

Figure 23 Energy diagram for Nb_3O_7OH and Pt Nanoparticles.

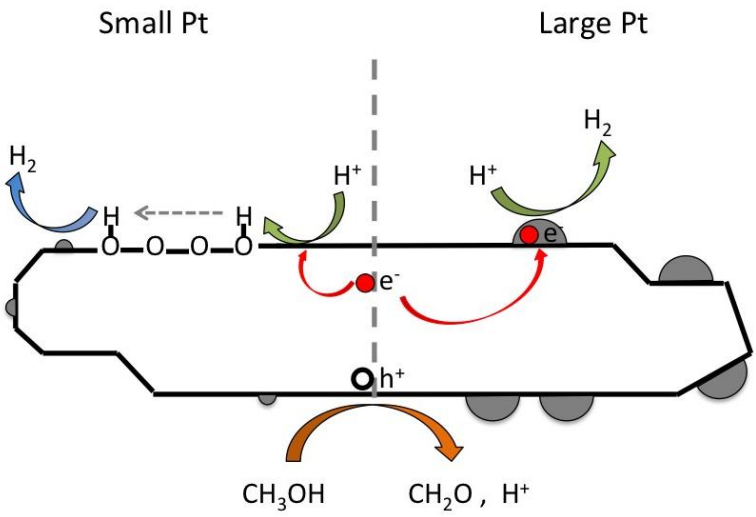

Figure 24 Proposed reaction mechanism for low platinum loading (left), involving reverse hydrogen spillover and high platinum loading (right) involving electron transfer to the metal particle and subsequent proton reduction.

These findings can help to further rationalize the development of efficient photocatalytic hydrogen evolution systems; highlighting the importance of semiconductor surface reaction, even in semiconductor/metal heterostructures where the fast electron transfer to the metal particle was believed to be the predominant mechanism

CHAPTER IV

PHOTOCATALYTIC PROPERTIES OF PHOTODEPOSITED AU, AG, PD AND CU NANOPARTICLES ON THE SURFACE OF NB_3O_7OH

A. Results and Discussion

1. Powder X-ray Diffraction

The PXRD patterns **(Figure 25)** clearly show that the experimental peaks of the decorated compounds are in agreement with the peaks of the pure non-decorated Nb_3O_7OH. This proves the phase purity of the compounds and that the crystallinity of Nb_3O_7OH was not affected by loading the metals.

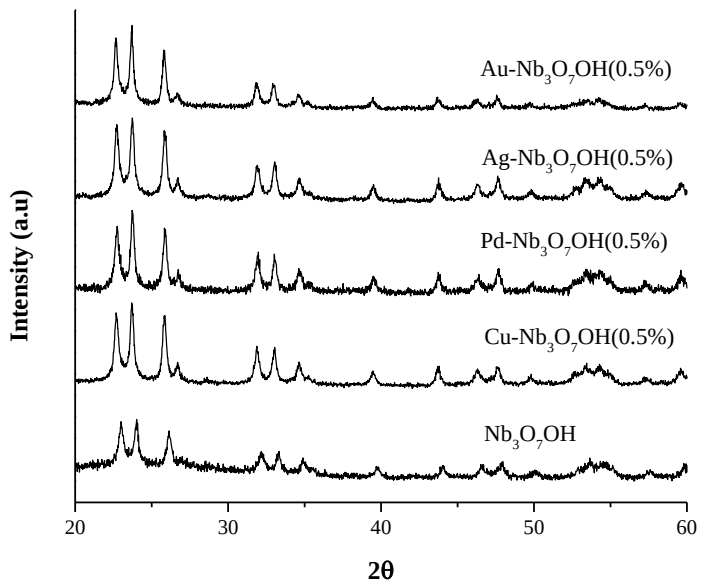

Figure 25 Layered Powder X-ray diffraction of all compounds with 0.5% metal loading with pure Nb_3O_7OH as reference.

2. *Scanning Electron microscopy imaging:*

High magnification SEM images are shown here, display the uniform shape of the decorated nanorods. We can also see clearly the small Nps on the nanorod surfaces (**Figure. 26**).

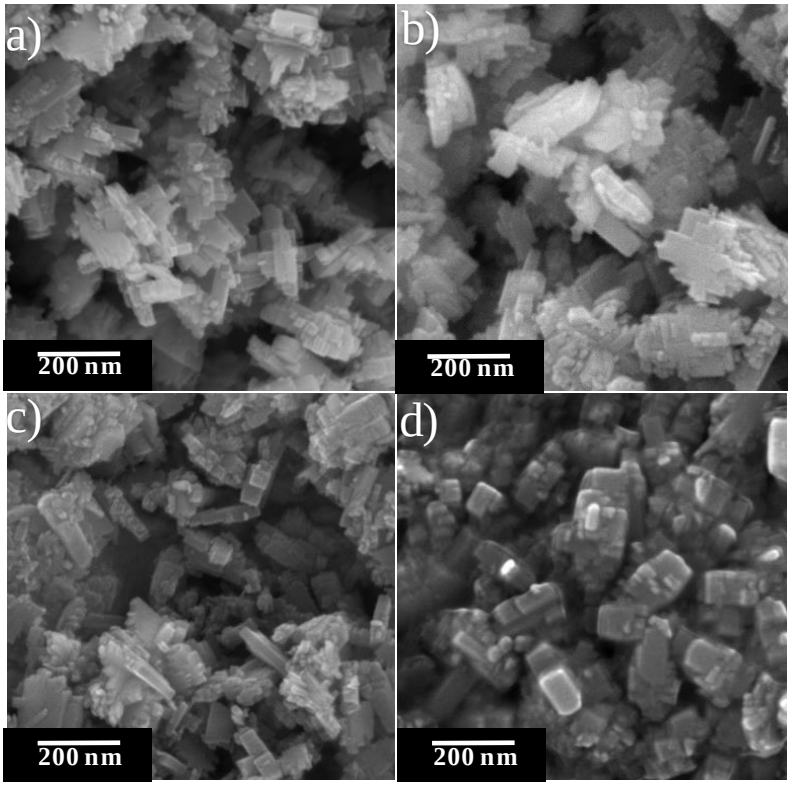

Figure 26 SEM images of (a) Cu- Nb_3O_7OH (0.5%) (b) Pd- Nb_3O_7OH (0.5%) (c) Ag- Nb_3O_7OH (0.5%) and (d) Au- Nb_3O_7OH (0.5%).

3. *EDX and Atomic absorption:*

Atomic absorption was performed on the synthesized compounds to detect the effective loading percentage of each metal on each catalyst. The data shows clearly the successful deposition of the metals on the surface of the catalyst. It is important to mention that, as expected, EDX results are less accurate than AA (**Table 2** and **Table**

3). Also, the results of AA are in close agreement with the expected weight percentage from each synthesis except for Cu.

Compound	**Atomic Absorption**	**EDX**
Cu- Nb_3O_7OH(5%)	2.85 %	9.06 %
Pd- Nb_3O_7OH(5%)	4.87 %	3.02 %
Ag- Nb_3O_7OH(5%)	4.53 %	5.96 %
Au- Nb_3O_7OH(5%)	4.00 %	3.1 %

Table 2 A comparison between the results of Atomic Absorption and EDX for the determination of the metal loading on the surface of Nb_3O_7OH in the case of 5% initial loading (results are shown in weight percent).

Compound	**Atomic Absorption**	**EDX**
Pd- Nb_3O_7OH(0.5%)	0.39 %	0.71 %
Ag- Nb_3O_7OH(0.5%)	0.55 %	0.41 %
Au- Nb_3O_7OH(0.5%)	0.47 %	0.10 %

Table 3 A comparison between the results of Atomic Absorption and EDX for the determination of the metal loading on the surface of Nb_3O_7OH in the case of 0.5% initial loading (results are shown in weight percent).

4. Photocatalytic activity of the heteronanostructures:

Rhodamine B is extensively used as a textiles colorant and foodstuffs. Also, it is well-known as a fluorescent water tracer.[170] Nevertheless, it is damaging to humans and animals and can cause respiratory, eye, and skin irritations. Also, it is well established that Rhodamine B has carcinogenic, reproductive, developmental, neuronal, and chronic toxicity hazards.[171, 172] Therefore, being aware of those mentioned hazards, it is worth trying to degrade Rhodamine B is present in an aqueous medium using our developed photocatalysts.

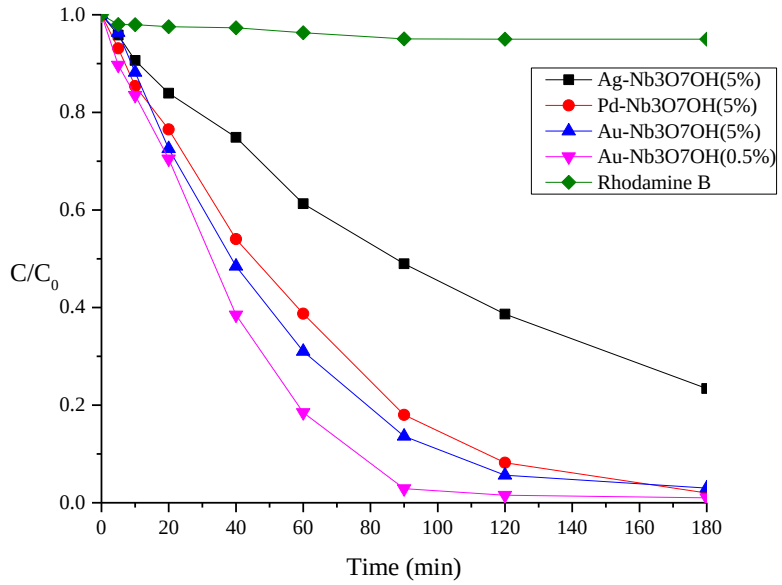

Figure 27 Relative concentration of Rhodamine B vs. duration of irradiation for each of the tested catalysts. A graph for Rhodamine B alone without any catalyst is also shown.

We can see from the results (**Figure. 27**) that the best compound yet is the gold decorated compound with a percent loading of 0.5%. This demonstrates that there is a better electrons-hole separation at the surface of the catalyst in the case of Au NPs.

CHAPTER V

CONCLUSION

In this work, we reviewed the concept of photocatalysis of the semiconductors, the challenges imposed and the strategies used to increase their efficiency. We then successfully synthesized and characterized new heteronanostructured samples of the semiconductor Nb_3O_7OH decorated with different metal loadings of Pt, Au, Cu, Pd, and Ag via a photodeposition technique. The compounds were characterized by XRD, SEM, EDX, TEM, and Atomic absorption.

In the first project, using the Pt decorated $Nb_3O_7(OH)$ photocatalyst, we investigated the effect of Pt loading on the catalytic H_2 production. Using XPS measurements, the obtained results showed that the reverse spillover mechanism is dominant at low Pt loading and it correlated with the highest H_2 production rate. On the other hand, at high Pt loading, the charge transfer mechanism was dominant and the production of H_2 decreased.

In the second project, we synthesized several new heteronanostructures of $Nb_3O_7(OH)$ decorated with Cu, Pd, Au, and Ag via the photodepositon method. Then, we studied their activity in the photocatalytic degradation of the toxic dye Rhodamine B. The best one of the tested compounds till now is the gold decorated compound with 0.5% as metal loading.

CHAPTER VI

FUTURE PERSPECTIVE

In the future, we would like to study the photocatalytic reaction mechanism lying behind the Rhodamine B degradation. This will be investigated further by using different hole scavengers in order to know the active species responsible for the degradation. In addition, we will explore the synthesized photocatalysts for alternative photocatalytic reactions: CO_2 reduction, degradation of drugs. Finally, it would be interesting to study the anionic and/or cationic doping of $Nb_3O_7(OH)$ to tune the bandgap and the band edge positions for enhanced photocatalytic activities.

REFERENCES

1. Zhou, H.; Qu, Y.; Zeid, T.; Duan, X., Towards highly efficient photocatalysts using semiconductor nanoarchitectures. *Energy & Environmental Science* **2012,** *5* (5), 6732-6743.
2. Lewis, N. S.; Nocera, D. G., Powering the planet: Chemical challenges in solar energy utilization. *Proceedings of the National Academy of Sciences* **2006,** *103* (43), 15729-15735.
3. Fan, W.; Zhang, Q.; Wang, Y., Semiconductor-based nanocomposites for photocatalytic H2 production and CO2 conversion. *Physical Chemistry Chemical Physics* **2013,** *15* (8), 2632-2649.
4. Sakakura, T.; Choi, J.-C.; Yasuda, H., Transformation of Carbon Dioxide. *Chemical Reviews* **2007,** *107* (6), 2365-2387.
5. Hunt, A. J.; Sin, E. H. K.; Marriott, R.; Clark, J. H., Generation, Capture, and Utilization of Industrial Carbon Dioxide. *ChemSusChem* **2010,** *3* (3), 306-322.
6. Cokoja, M.; Bruckmeier, C.; Rieger, B.; Herrmann, W. A.; Kühn, F. E., Transformation of Carbon Dioxide with Homogeneous Transition-Metal Catalysts: A Molecular Solution to a Global Challenge? *Angewandte Chemie International Edition* **2011,** *50* (37), 8510-8537.
7. Fujishima, A.; Honda, K., Electrochemical Photolysis of Water at a Semiconductor Electrode. *Nature* **1972,** *238* (5358), 37-38.
8. Inoue, T.; Fujishima, A.; Konishi, S.; Honda, K., Photoelectrocatalytic reduction of carbon dioxide in aqueous suspensions of semiconductor powders. *Nature* **1979,** *277* (5698), 637-638.
9. Korzhak, A. V.; Ermokhina, N. I.; Stroyuk, A. L.; Bukhtiyarov, V. K.; Raevskaya, A. E.; Litvin, V. I.; Kuchmiy, S. Y.; Ilyin, V. G.; Manorik, P. A., Photocatalytic hydrogen evolution over mesoporous TiO2/metal nanocomposites. *Journal of Photochemistry and Photobiology A: Chemistry* **2008,** *198* (2), 126-134.
10. Lou, X. W.; Archer, L. A.; Yang, Z., Hollow Micro-/Nanostructures: Synthesis and Applications. *Advanced Materials* **2008,** *20* (21), 3987-4019.
11. Li, Y.; Sasaki, T.; Shimizu, Y.; Koshizaki, N., Hexagonal-Close-Packed, Hierarchical Amorphous TiO2 Nanocolumn Arrays: Transferability, Enhanced Photocatalytic Activity, and Superamphiphilicity without UV Irradiation. *Journal of the American Chemical Society* **2008,** *130* (44), 14755-14762.
12. Wang, X. D.; Summers, C. J.; Wang, Z. L., Mesoporous Single-Crystal ZnO Nanowires Epitaxially Sheathed with Zn2SiO4. *Advanced Materials* **2004,** *16* (14), 1215-1218.
13. Kochuveedu, S. T.; Jang, Y. H.; Kim, D. H., A study on the mechanism for the interaction of light with noble metal-metal oxide semiconductor nanostructures for various photophysical applications. *Chemical Society Reviews* **2013,** *42* (21), 8467-8493.
14. Bard, A. J.; Fox, M. A., Artificial Photosynthesis: Solar Splitting of Water to Hydrogen and Oxygen. *Accounts of Chemical Research* **1995,** *28* (3), 141-145.
15. Baxter, J. B.; Richter, C.; Schmuttenmaer, C. A., Ultrafast Carrier Dynamics in Nanostructures for Solar Fuels. *Annual Review of Physical Chemistry* **2014,** *65* (1), 423-447.
16. Zhen, C.; Wang, L.; Liu, G.; Lu, G. Q.; Cheng, H.-M., Template-free synthesis of Ta3N5 nanorod arrays for efficient photoelectrochemical water splitting. *Chemical Communications* **2013,** *49* (29), 3019-3021.
17. Yan, S.; Wan, L.; Li, Z.; Zou, Z., Facile temperature-controlled synthesis of hexagonal Zn2GeO4 nanorods with different aspect ratios toward improved photocatalytic activity for overall water splitting and photoreduction of CO2. *Chemical Communications* **2011,** *47* (19), 5632-5634.
18. Chen, S.; Huang, D.; Xu, P.; Xue, W.; Lei, L.; Cheng, M.; Wang, R.; Liu, X.; Deng, R., Semiconductor-based photocatalysts for photocatalytic and photoelectrochemical water splitting: will we stop with photocorrosion? *Journal of Materials Chemistry A* **2020,** *8* (5), 2286-2322.

19. Sun, S.; Wang, W.; Li, D.; Zhang, L.; Jiang, D., Solar Light Driven Pure Water Splitting on Quantum Sized BiVO4 without any Cocatalyst. *ACS Catalysis* **2014,** *4* (10), 3498-3503.
20. Li, Z.; Luo, W.; Zhang, M.; Feng, J.; Zou, Z., Photoelectrochemical cells for solar hydrogen production: current state of promising photoelectrodes, methods to improve their properties, and outlook. *Energy & Environmental Science* **2013,** *6* (2), 347-370.
21. Ager, J. W.; Shaner, M. R.; Walczak, K. A.; Sharp, I. D.; Ardo, S., Experimental demonstrations of spontaneous, solar-driven photoelectrochemical water splitting. *Energy & Environmental Science* **2015,** *8* (10), 2811-2824.
22. Fujishima, A.; Zhang, X.; Tryk, D. A., TiO2 photocatalysis and related surface phenomena. *Surface Science Reports* **2008,** *63* (12), 515-582.
23. Gueymard, C. A., The sun's total and spectral irradiance for solar energy applications and solar radiation models. *Solar Energy* **2004,** *76* (4), 423-453.
24. Ni, M.; Leung, M. K. H.; Leung, D. Y. C.; Sumathy, K., A review and recent developments in photocatalytic water-splitting using TiO2 for hydrogen production. *Renewable and Sustainable Energy Reviews* **2007,** *11* (3), 401-425.
25. Choi, J.; Park, H.; Hoffmann, M. R., Effects of Single Metal-Ion Doping on the Visible-Light Photoreactivity of TiO2. *The Journal of Physical Chemistry C* **2010,** *114* (2), 783-792.
26. Kang, Z.; Liu, Y.; Tsang, C. H. A.; Ma, D. D. D.; Fan, X.; Wong, N.-B.; Lee, S.-T., Water-Soluble Silicon Quantum Dots with Wavelength-Tunable Photoluminescence. *Advanced Materials* **2009,** *21* (6), 661-664.
27. Ohmori, T.; Mametsuka, H.; Suzuki, E., Photocatalytic hydrogen evolution on InP suspension with inorganic sacrificial reducing agent. *International Journal of Hydrogen Energy* **2000,** *25* (10), 953-955.
28. Costi, R.; Cohen, G.; Salant, A.; Rabani, E.; Banin, U., Electrostatic Force Microscopy Study of Single Au−CdSe Hybrid Nanodumbbells: Evidence for Light-Induced Charge Separation. *Nano Letters* **2009,** *9* (5), 2031-2039.
29. Maeda, K.; Takata, T.; Hara, M.; Saito, N.; Inoue, Y.; Kobayashi, H.; Domen, K., GaN:ZnO Solid Solution as a Photocatalyst for Visible-Light-Driven Overall Water Splitting. *Journal of the American Chemical Society* **2005,** *127* (23), 8286-8287.
30. Maeda, K.; Teramura, K.; Lu, D.; Takata, T.; Saito, N.; Inoue, Y.; Domen, K., Photocatalyst releasing hydrogen from water. *Nature* **2006,** *440* (7082), 295-295.
31. Tryk, D. A.; Fujishima, A.; Honda, K., Recent topics in photoelectrochemistry: achievements and future prospects. *Electrochimica Acta* **2000,** *45* (15), 2363-2376.
32. Li, D.; Haneda, H.; Labhsetwar, N. K.; Hishita, S.; Ohashi, N., Visible-light-driven photocatalysis on fluorine-doped TiO2 powders by the creation of surface oxygen vacancies. *Chemical Physics Letters* **2005,** *401* (4), 579-584.
33. Linsebigler, A. L.; Lu, G.; Yates, J. T., Photocatalysis on TiO2 Surfaces: Principles, Mechanisms, and Selected Results. *Chemical Reviews* **1995,** *95* (3), 735-758.
34. Zhang, J.; Wu, Y.; Xing, M.; Leghari, S. A. K.; Sajjad, S., Development of modified N doped TiO2 photocatalyst with metals, nonmetals and metal oxides. *Energy & Environmental Science* **2010,** *3* (6), 715-726.
35. Chen, X.; Liu, L.; Yu, P. Y.; Mao, S. S., Increasing Solar Absorption for Photocatalysis with Black Hydrogenated Titanium Dioxide Nanocrystals. *Science* **2011,** *331* (6018), 746.
36. Kudo, A.; Miseki, Y., Heterogeneous photocatalyst materials for water splitting. *Chemical Society Reviews* **2009,** *38* (1), 253-278.
37. Wang, G.; Wang, H.; Ling, Y.; Tang, Y.; Yang, X.; Fitzmorris, R. C.; Wang, C.; Zhang, J. Z.; Li, Y., Hydrogen-Treated TiO2 Nanowire Arrays for Photoelectrochemical Water Splitting. *Nano Letters* **2011,** *11* (7), 3026-3033.
38. Jing, L.; Zhou, W.; Tian, G.; Fu, H., Surface tuning for oxide-based nanomaterials as efficient photocatalysts. *Chemical Society Reviews* **2013,** *42* (24), 9509-9549.
39. Maeda, K.; Xiong, A.; Yoshinaga, T.; Ikeda, T.; Sakamoto, N.; Hisatomi, T.; Takashima, M.; Lu, D.; Kanehara, M.; Setoyama, T.; Teranishi, T.; Domen, K., Photocatalytic Overall Water Splitting Promoted by Two Different Cocatalysts for Hydrogen and Oxygen

Evolution under Visible Light. *Angewandte Chemie International Edition* **2010,** *49* (24), 4096-4099.
40. Ning, Z.; Tian, H.; Yuan, C.; Fu, Y.; Qin, H.; Sun, L.; Ågren, H., Solar cells sensitized with type-II ZnSe–CdS core/shell colloidal quantum dots. *Chemical Communications* **2011,** *47* (5), 1536-1538.
41. Brahimi, R.; Bessekhouad, Y.; Bouguelia, A.; Trari, M., Improvement of eosin visible light degradation using PbS-sensititized TiO2. *Journal of Photochemistry and Photobiology A: Chemistry* **2008,** *194* (2), 173-180.
42. Ho, W.; Yu, J. C., Sonochemical synthesis and visible light photocatalytic behavior of CdSe and CdSe/TiO2 nanoparticles. *Journal of Molecular Catalysis A: Chemical* **2006,** *247* (1), 268-274.
43. Kongkanand, A.; Tvrdy, K.; Takechi, K.; Kuno, M.; Kamat, P. V., Quantum Dot Solar Cells. Tuning Photoresponse through Size and Shape Control of CdSe−TiO2 Architecture. *Journal of the American Chemical Society* **2008,** *130* (12), 4007-4015.
44. Nedeljković, J. M.; Mićić, O. I.; Ahrenkiel, S. P.; Miedaner, A.; Nozik, A. J., Growth of InP Nanostructures via Reaction of Indium Droplets with Phosphide Ions: Synthesis of InP Quantum Rods and InP−TiO2 Composites. *Journal of the American Chemical Society* **2004,** *126* (8), 2632-2639.
45. Hu, C.; Guo, J.; Qu, J.; Hu, X., Photocatalytic Degradation of Pathogenic Bacteria with AgI/TiO2 under Visible Light Irradiation. *Langmuir* **2007,** *23* (9), 4982-4987.
46. Li, Y.; Zhang, H.; Guo, Z.; Han, J.; Zhao, X.; Zhao, Q.; Kim, S.-J., Highly Efficient Visible-Light-Induced Photocatalytic Activity of Nanostructured AgI/TiO2 Photocatalyst. *Langmuir* **2008,** *24* (15), 8351-8357.
47. Niu, M.; Huang, F.; Cui, L.; Huang, P.; Yu, Y.; Wang, Y., Hydrothermal Synthesis, Structural Characteristics, and Enhanced Photocatalysis of SnO2/α-Fe2O3 Semiconductor Nanoheterostructures. *ACS Nano* **2010,** *4* (2), 681-688.
48. Cao, T.; Li, Y.; Wang, C.; Wei, L.; Shao, C.; Liu, Y., Fabrication, structure, and enhanced photocatalytic properties of hierarchical CeO2 nanostructures/TiO2 nanofibers heterostructures. *Materials Research Bulletin* **2010,** *45* (10), 1406-1412.
49. Amirav, L.; Alivisatos, A. P., Photocatalytic Hydrogen Production with Tunable Nanorod Heterostructures. *The Journal of Physical Chemistry Letters* **2010,** *1* (7), 1051-1054.
50. Banerjee, S.; Mohapatra, S. K.; Das, P. P.; Misra, M., Synthesis of Coupled Semiconductor by Filling 1D TiO2 Nanotubes with CdS. *Chemistry of Materials* **2008,** *20* (21), 6784-6791.
51. Ratanatawanate, C.; Tao, Y.; Balkus, K. J., Photocatalytic Activity of PbS Quantum Dot/TiO2 Nanotube Composites. *The Journal of Physical Chemistry C* **2009,** *113* (24), 10755-10760.
52. Chen, F.; Deng, Z.; Li, X.; Zhang, J.; Zhao, J., Visible light detoxification by 2,9,16,23-tetracarboxyl phthalocyanine copper modified amorphous titania. *Chemical Physics Letters* **2005,** *415* (1), 85-88.
53. Nazeeruddin, M. K.; De Angelis, F.; Fantacci, S.; Selloni, A.; Viscardi, G.; Liska, P.; Ito, S.; Takeru, B.; Grätzel, M., Combined Experimental and DFT-TDDFT Computational Study of Photoelectrochemical Cell Ruthenium Sensitizers. *Journal of the American Chemical Society* **2005,** *127* (48), 16835-16847.
54. O'Regan, B.; Grätzel, M., A low-cost, high-efficiency solar cell based on dye-sensitized colloidal TiO2 films. *Nature* **1991,** *353* (6346), 737-740.
55. Wang, P.; Dai, Q.; Zakeeruddin, S. M.; Forsyth, M.; MacFarlane, D. R.; Grätzel, M., Ambient Temperature Plastic Crystal Electrolyte for Efficient, All-Solid-State Dye-Sensitized Solar Cell. *Journal of the American Chemical Society* **2004,** *126* (42), 13590-13591.
56. Robertson, N., Catching the Rainbow: Light Harvesting in Dye-Sensitized Solar Cells. *Angewandte Chemie International Edition* **2008,** *47* (6), 1012-1014.
57. Michael, G., Mesoscopic Solar Cells for Electricity and Hydrogen Production from Sunlight. *Chemistry Letters* **2005,** *34* (1), 8-13.

58. Maeda, K.; Eguchi, M.; Youngblood, W. J.; Mallouk, T. E., Niobium Oxide Nanoscrolls as Building Blocks for Dye-Sensitized Hydrogen Production from Water under Visible Light Irradiation. *Chemistry of Materials* **2008,** *20* (21), 6770-6778.
59. Moores, A.; Goettmann, F., The plasmon band in noble metal nanoparticles: an introduction to theory and applications. *New Journal of Chemistry* **2006,** *30* (8), 1121-1132.
60. Schwartzberg, A. M.; Zhang, J. Z., Novel Optical Properties and Emerging Applications of Metal Nanostructures. *The Journal of Physical Chemistry C* **2008,** *112* (28), 10323-10337.
61. Stewart, M. E.; Anderton, C. R.; Thompson, L. B.; Maria, J.; Gray, S. K.; Rogers, J. A.; Nuzzo, R. G., Nanostructured Plasmonic Sensors. *Chemical Reviews* **2008,** *108* (2), 494-521.
62. Murray, W. A.; Barnes, W. L., Plasmonic Materials. *Advanced Materials* **2007,** *19* (22), 3771-3782.
63. Barnes, W. L.; Dereux, A.; Ebbesen, T. W., Surface plasmon subwavelength optics. *Nature* **2003,** *424* (6950), 824-830.
64. Eustis, S.; El-Sayed, M. A., Why gold nanoparticles are more precious than pretty gold: Noble metal surface plasmon resonance and its enhancement of the radiative and nonradiative properties of nanocrystals of different shapes. *Chemical Society Reviews* **2006,** *35* (3), 209-217.
65. Kelly, K. L.; Coronado, E.; Zhao, L. L.; Schatz, G. C., The Optical Properties of Metal Nanoparticles: The Influence of Size, Shape, and Dielectric Environment. *The Journal of Physical Chemistry B* **2003,** *107* (3), 668-677.
66. Tsukamoto, D.; Shiraishi, Y.; Sugano, Y.; Ichikawa, S.; Tanaka, S.; Hirai, T., Gold Nanoparticles Located at the Interface of Anatase/Rutile TiO2 Particles as Active Plasmonic Photocatalysts for Aerobic Oxidation. *Journal of the American Chemical Society* **2012,** *134* (14), 6309-6315.
67. Ide, Y.; Matsuoka, M.; Ogawa, M., Efficient Visible-Light-Induced Photocatalytic Activity on Gold-Nanoparticle-Supported Layered Titanate. *Journal of the American Chemical Society* **2010,** *132* (47), 16762-16764.
68. Seh, Z. W.; Liu, S.; Low, M.; Zhang, S.-Y.; Liu, Z.; Mlayah, A.; Han, M.-Y., Janus Au-TiO2 Photocatalysts with Strong Localization of Plasmonic Near-Fields for Efficient Visible-Light Hydrogen Generation. *Advanced Materials* **2012,** *24* (17), 2310-2314.
69. Jain, P. K.; Huang, X.; El-Sayed, I. H.; El-Sayed, M. A., Noble Metals on the Nanoscale: Optical and Photothermal Properties and Some Applications in Imaging, Sensing, Biology, and Medicine. *Accounts of Chemical Research* **2008,** *41* (12), 1578-1586.
70. Law, W.-C.; Yong, K.-T.; Baev, A.; Prasad, P. N., Sensitivity Improved Surface Plasmon Resonance Biosensor for Cancer Biomarker Detection Based on Plasmonic Enhancement. *ACS Nano* **2011,** *5* (6), 4858-4864.
71. Prabhakar, N.; Arora, K.; Arya, S. K.; Solanki, P. R.; Iwamoto, M.; Singh, H.; Malhotra, B. D., Nucleic acid sensor for M. tuberculosis detection based on surface plasmon resonance. *Analyst* **2008,** *133* (11), 1587-1592.
72. Standridge, S. D.; Schatz, G. C.; Hupp, J. T., Distance Dependence of Plasmon-Enhanced Photocurrent in Dye-Sensitized Solar Cells. *Journal of the American Chemical Society* **2009,** *131* (24), 8407-8409.
73. Brown, M. D.; Suteewong, T.; Kumar, R. S. S.; D'Innocenzo, V.; Petrozza, A.; Lee, M. M.; Wiesner, U.; Snaith, H. J., Plasmonic Dye-Sensitized Solar Cells Using Core−Shell Metal−Insulator Nanoparticles. *Nano Letters* **2011,** *11* (2), 438-445.
74. Atwater, H. A.; Polman, A., Plasmonics for improved photovoltaic devices. In *Materials for Sustainable Energy*, Co-Published with Macmillan Publishers Ltd, UK: 2010; pp 1-11.
75. Camden, J. P.; Dieringer, J. A.; Zhao, J.; Van Duyne, R. P., Controlled Plasmonic Nanostructures for Surface-Enhanced Spectroscopy and Sensing. *Accounts of Chemical Research* **2008,** *41* (12), 1653-1661.
76. Brus, L., Noble Metal Nanocrystals: Plasmon Electron Transfer Photochemistry and Single-Molecule Raman Spectroscopy. *Accounts of Chemical Research* **2008,** *41* (12), 1742-1749.

77. Li, X.; Hu, H.; Li, D.; Shen, Z.; Xiong, Q.; Li, S.; Fan, H. J., Ordered Array of Gold Semishells on TiO2 Spheres: An Ultrasensitive and Recyclable SERS Substrate. *ACS Applied Materials & Interfaces* **2012,** *4* (4), 2180-2185.
78. Kamat, P. V., Photophysical, Photochemical and Photocatalytic Aspects of Metal Nanoparticles. *The Journal of Physical Chemistry B* **2002,** *106* (32), 7729-7744.
79. Zhang, Q.; Lima, D. Q.; Lee, I.; Zaera, F.; Chi, M.; Yin, Y., A Highly Active Titanium Dioxide Based Visible-Light Photocatalyst with Nonmetal Doping and Plasmonic Metal Decoration. *Angewandte Chemie International Edition* **2011,** *50* (31), 7088-7092.
80. Zheng, Z.; Huang, B.; Qin, X.; Zhang, X.; Dai, Y.; Whangbo, M.-H., Facile in situ synthesis of visible-light plasmonic photocatalysts M@TiO2 (M = Au, Pt, Ag) and evaluation of their photocatalytic oxidation of benzene to phenol. *Journal of Materials Chemistry* **2011,** *21* (25), 9079-9087.
81. Kochuveedu, S. T.; Kim, D.-P.; Kim, D. H., Surface-Plasmon-Induced Visible Light Photocatalytic Activity of TiO2 Nanospheres Decorated by Au Nanoparticles with Controlled Configuration. *The Journal of Physical Chemistry C* **2012,** *116* (3), 2500-2506.
82. Elmoula, M. A.; Panaitescu, E.; Phan, M.; Yin, D.; Richter, C.; Lewis, L. H.; Menon, L., Controlled attachment of gold nanoparticles on ordered titania nanotube arrays. *Journal of Materials Chemistry* **2009,** *19* (26), 4483-4487.
83. Zheng, Z.; Teo, J.; Chen, X.; Liu, H.; Yuan, Y.; Waclawik, E. R.; Zhong, Z.; Zhu, H., Correlation of the Catalytic Activity for Oxidation Taking Place on Various TiO2 Surfaces with Surface OH Groups and Surface Oxygen Vacancies. *Chemistry – A European Journal* **2010,** *16* (4), 1202-1211.
84. Rodríguez-González, V.; Zanella, R.; del Angel, G.; Gómez, R., MTBE visible-light photocatalytic decomposition over Au/TiO2 and Au/TiO2–Al2O3 sol–gel prepared catalysts. *Journal of Molecular Catalysis A: Chemical* **2008,** *281* (1), 93-98.
85. Chen, J.-J.; Wu, J. C. S.; Wu, P. C.; Tsai, D. P., Plasmonic Photocatalyst for H2 Evolution in Photocatalytic Water Splitting. *The Journal of Physical Chemistry C* **2011,** *115* (1), 210-216.
86. Kiyonaga, T.; Jin, Q.; Kobayashi, H.; Tada, H., Size-Dependence of Catalytic Activity of Gold Nanoparticles Loaded on Titanium (IV) Dioxide for Hydrogen Peroxide Decomposition. *ChemPhysChem* **2009,** *10* (17), 2935-2938.
87. Kimura, K.; Naya, S.-i.; Jin-nouchi, Y.; Tada, H., TiO2 Crystal Form-Dependence of the Au/TiO2 Plasmon Photocatalyst's Activity. *The Journal of Physical Chemistry C* **2012,** *116* (12), 7111-7117.
88. Kowalska, E.; Abe, R.; Ohtani, B., Visible light-induced photocatalytic reaction of gold-modified titanium(iv) oxide particles: action spectrum analysis. *Chemical Communications* **2009,** (2), 241-243.
89. Kowalska, E.; Rau, S.; Ohtani, B., Plasmonic Titania Photocatalysts Active under UV and Visible-Light Irradiation: Influence of Gold Amount, Size, and Shape. *Journal of Nanotechnology* **2012,** *2012*, 361853.
90. Wu, Y.; Liu, H.; Zhang, J.; Chen, F., Enhanced Photocatalytic Activity of Nitrogen-Doped Titania by Deposited with Gold. *The Journal of Physical Chemistry C* **2009,** *113* (33), 14689-14695.
91. Gomes Silva, C.; Juárez, R.; Marino, T.; Molinari, R.; García, H., Influence of Excitation Wavelength (UV or Visible Light) on the Photocatalytic Activity of Titania Containing Gold Nanoparticles for the Generation of Hydrogen or Oxygen from Water. *Journal of the American Chemical Society* **2011,** *133* (3), 595-602.
92. Pandikumar, A.; Manonmani, S.; Ramaraj, R., TiO2–Au nanocomposite materials embedded in polymer matrices and their application in the photocatalytic reduction of nitrite to ammonia. *Catalysis Science & Technology* **2012,** *2* (2), 345-353.
93. Kowalska, E.; Mahaney, O. O. P.; Abe, R.; Ohtani, B., Visible-light-induced photocatalysis through surface plasmon excitation of gold on titania surfaces. *Physical Chemistry Chemical Physics* **2010,** *12* (10), 2344-2355.

94. Hou, W.; Liu, Z.; Pavaskar, P.; Hung, W. H.; Cronin, S. B., Plasmonic enhancement of photocatalytic decomposition of methyl orange under visible light. *Journal of Catalysis* **2011,** *277* (2), 149-153.
95. Liu, Z.; Hou, W.; Pavaskar, P.; Aykol, M.; Cronin, S. B., Plasmon Resonant Enhancement of Photocatalytic Water Splitting Under Visible Illumination. *Nano Letters* **2011,** *11* (3), 1111-1116.
96. Tian, Y.; Tatsuma, T., Mechanisms and Applications of Plasmon-Induced Charge Separation at TiO2 Films Loaded with Gold Nanoparticles. *Journal of the American Chemical Society* **2005,** *127* (20), 7632-7637.
97. Lu, Y.; Yu, H.; Chen, S.; Quan, X.; Zhao, H., Integrating Plasmonic Nanoparticles with TiO2 Photonic Crystal for Enhancement of Visible-Light-Driven Photocatalysis. *Environmental Science & Technology* **2012,** *46* (3), 1724-1730.
98. Liu, Y.; Shu, W.; Peng, Z.; Chen, K.; Chen, W., Self-assembly of Au nanocrystal/titanate nanobelt heterojunctions and enhancement of the photocatalytic activity. *Catalysis Today* **2013,** *208*, 28-34.
99. Li, H.; Bian, Z.; Zhu, J.; Huo, Y.; Li, H.; Lu, Y., Mesoporous Au/TiO2 Nanocomposites with Enhanced Photocatalytic Activity. *Journal of the American Chemical Society* **2007,** *129* (15), 4538-4539.
100. Zhou, M.; Zhang, J.; Cheng, B.; Yu, H., Enhancement of Visible-Light Photocatalytic Activity of Mesoporous Au-TiO₂ Nanocomposites by Surface Plasmon Resonance. *International Journal of Photoenergy* **2012,** *2012*, 532843.
101. Ingram, D. B.; Linic, S., Water Splitting on Composite Plasmonic-Metal/Semiconductor Photoelectrodes: Evidence for Selective Plasmon-Induced Formation of Charge Carriers near the Semiconductor Surface. *Journal of the American Chemical Society* **2011,** *133* (14), 5202-5205.
102. Li, M.; Wang, R.; Zhong, P.; Li, X.; Huang, Z.; Zhang, C., Ag–TiO2–Ag core–shell–satellite nanowires: Facile synthesis and enhanced photocatalytic activities. *Materials Letters* **2012,** *80*, 138-140.
103. Ingram, D. B.; Christopher, P.; Bauer, J. L.; Linic, S., Predictive Model for the Design of Plasmonic Metal/Semiconductor Composite Photocatalysts. *ACS Catalysis* **2011,** *1* (10), 1441-1447.
104. Jiang, L.; Zhou, G.; Mi, J.; Wu, Z., Fabrication of visible-light-driven one-dimensional anatase TiO2/Ag heterojunction plasmonic photocatalyst. *Catalysis Communications* **2012,** *24*, 48-51.
105. Sauthier, G.; Pérez del Pino, A.; Figueras, A.; György, E., Synthesis and Characterization of Ag Nanoparticles and Ag-Loaded TiO2 Photocatalysts. *Journal of the American Ceramic Society* **2011,** *94* (11), 3780-3786.
106. Akhavan, O., Lasting antibacterial activities of Ag–TiO2/Ag/a-TiO2 nanocomposite thin film photocatalysts under solar light irradiation. *Journal of Colloid and Interface Science* **2009,** *336* (1), 117-124.
107. Sangpour, P.; Hashemi, F.; Moshfegh, A. Z., Photoenhanced Degradation of Methylene Blue on Cosputtered M:TiO2 (M = Au, Ag, Cu) Nanocomposite Systems: A Comparative Study. *The Journal of Physical Chemistry C* **2010,** *114* (33), 13955-13961.
108. Zhou, X.; Liu, G.; Yu, J.; Fan, W., Surface plasmon resonance-mediated photocatalysis by noble metal-based composites under visible light. *Journal of Materials Chemistry* **2012,** *22* (40), 21337-21354.
109. Furube, A.; Du, L.; Hara, K.; Katoh, R.; Tachiya, M., Ultrafast Plasmon-Induced Electron Transfer from Gold Nanodots into TiO2 Nanoparticles. *Journal of the American Chemical Society* **2007,** *129* (48), 14852-14853.
110. Tang, Y.; Jiang, Z.; Tay, Q.; Deng, J.; Lai, Y.; Gong, D.; Dong, Z.; Chen, Z., Visible-light plasmonic photocatalyst anchored on titanate nanotubes: a novel nanohybrid with synergistic effects of adsorption and degradation. *RSC Advances* **2012,** *2* (25), 9406-9414.

111. Alessandri, I.; Ferroni, M., Exploiting optothermal conversion for nanofabrication: site-selective generation of Au/TiO2 inverse opals. *Journal of Materials Chemistry* **2009,** *19* (42), 7990-7994.
112. Bian, Z.; Zhu, J.; Cao, F.; Lu, Y.; Li, H., In situ encapsulation of Au nanoparticles in mesoporous core–shell TiO2 microspheres with enhanced activity and durability. *Chemical Communications* **2009,** (25), 3789-3791.
113. Wang, H.; You, T.; Shi, W.; Li, J.; Guo, L., Au/TiO2/Au as a Plasmonic Coupling Photocatalyst. *The Journal of Physical Chemistry C* **2012,** *116* (10), 6490-6494.
114. Linic, S.; Christopher, P.; Ingram, D. B., Plasmonic-metal nanostructures for efficient conversion of solar to chemical energy. *Nature Materials* **2011,** *10* (12), 911-921.
115. Turkevich, J.; Stevenson, P. C.; Hillier, J., The formation of colloidal gold. *The Journal of Physical Chemistry* **1953,** *57* (7), 670-673.
116. Anger, P.; Bharadwaj, P.; Novotny, L., Enhancement and Quenching of Single-Molecule Fluorescence. *Physical Review Letters* **2006,** *96* (11), 113002.
117. Christopher, P.; Ingram, D. B.; Linic, S., Enhancing Photochemical Activity of Semiconductor Nanoparticles with Optically Active Ag Nanostructures: Photochemistry Mediated by Ag Surface Plasmons. *The Journal of Physical Chemistry C* **2010,** *114* (19), 9173-9177.
118. Evanoff Jr, D. D.; Chumanov, G., Synthesis and Optical Properties of Silver Nanoparticles and Arrays. *ChemPhysChem* **2005,** *6* (7), 1221-1231.
119. Singh, S.; Faraz, M.; Khare, N., Recent Advances in Semiconductor–Graphene and Semiconductor–Ferroelectric/Ferromagnetic Nanoheterostructures for Efficient Hydrogen Generation and Environmental Remediation. *ACS Omega* **2020,** *5* (21), 11874-11882.
120. Chen, X.; Shen, S.; Guo, L.; Mao, S. S., Semiconductor-based Photocatalytic Hydrogen Generation. *Chemical Reviews* **2010,** *110* (11), 6503-6570.
121. Roy, S. C.; Varghese, O. K.; Paulose, M.; Grimes, C. A., Toward Solar Fuels: Photocatalytic Conversion of Carbon Dioxide to Hydrocarbons. *ACS Nano* **2010,** *4* (3), 1259-1278.
122. Linsebigler, A. L.; Lu, G.; Yates Jr, J. T., Photocatalysis on TiO2 surfaces: principles, mechanisms, and selected results. *Chemical reviews* **1995,** *95* (3), 735-758.
123. Jakob, M.; Levanon, H.; Kamat, P. V., Charge Distribution between UV-Irradiated TiO2 and Gold Nanoparticles: Determination of Shift in the Fermi Level. *Nano Letters* **2003,** *3* (3), 353-358.
124. Wood, A.; Giersig, M.; Mulvaney, P., Fermi Level Equilibration in Quantum Dot−Metal Nanojunctions. *The Journal of Physical Chemistry B* **2001,** *105* (37), 8810-8815.
125. Habisreutinger, S. N.; Schmidt-Mende, L.; Stolarczyk, J. K., Photocatalytic Reduction of CO2 on TiO2 and Other Semiconductors. *Angewandte Chemie International Edition* **2013,** *52* (29), 7372-7408.
126. Young, C.; Lim, T. M.; Chiang, K.; Scott, J.; Amal, R., Photocatalytic oxidation of toluene and trichloroethylene in the gas-phase by metallised (Pt, Ag) titanium dioxide. *Applied Catalysis B: Environmental* **2008,** *78* (1), 1-10.
127. Zhang, Z.; Shao, C.; Li, X.; Wang, C.; Zhang, M.; Liu, Y., Electrospun Nanofibers of p-Type NiO/n-Type ZnO Heterojunctions with Enhanced Photocatalytic Activity. *ACS Applied Materials & Interfaces* **2010,** *2* (10), 2915-2923.
128. Hou, J.; Wang, Z.; Kan, W.; Jiao, S.; Zhu, H.; Kumar, R. V., Efficient visible-light-driven photocatalytic hydrogen production using CdS@TaON core–shell composites coupled with graphene oxide nanosheets. *Journal of Materials Chemistry* **2012,** *22* (15), 7291-7299.
129. Maeda, K., Photocatalytic water splitting using semiconductor particles: History and recent developments. *Journal of Photochemistry and Photobiology C: Photochemistry Reviews* **2011,** *12* (4), 237-268.
130. Xing, J.; Fang, W. Q.; Zhao, H. J.; Yang, H. G., FOCUS REVIEWS. *Chem. Asian J* **2012,** *7*, 642-657.

131. Tada, H.; Mitsui, T.; Kiyonaga, T.; Akita, T.; Tanaka, K., All-solid-state Z-scheme in CdS–Au–TiO2 three-component nanojunction system. *Nature Materials* **2006,** *5* (10), 782-786.
132. Xiang, Q.; Yu, J.; Jaroniec, M., Synergetic Effect of MoS2 and Graphene as Cocatalysts for Enhanced Photocatalytic H2 Production Activity of TiO2 Nanoparticles. *Journal of the American Chemical Society* **2012,** *134* (15), 6575-6578.
133. Kato, H.; Asakura, K.; Kudo, A., Highly Efficient Water Splitting into H2 and O2 over Lanthanum-Doped NaTaO3 Photocatalysts with High Crystallinity and Surface Nanostructure. *Journal of the American Chemical Society* **2003,** *125* (10), 3082-3089.
134. Bao, N.; Shen, L.; Takata, T.; Domen, K., Self-Templated Synthesis of Nanoporous CdS Nanostructures for Highly Efficient Photocatalytic Hydrogen Production under Visible Light. *Chemistry of Materials* **2008,** *20* (1), 110-117.
135. Zong, X.; Yan, H.; Wu, G.; Ma, G.; Wen, F.; Wang, L.; Li, C., Enhancement of Photocatalytic H2 Evolution on CdS by Loading MoS2 as Cocatalyst under Visible Light Irradiation. *Journal of the American Chemical Society* **2008,** *130* (23), 7176-7177.
136. Hu, X.; Cossairt, B. M.; Brunschwig, B. S.; Lewis, N. S.; Peters, J. C., Electrocatalytic hydrogen evolution by cobalt difluoroboryl-diglyoximate complexes. *Chemical Communications* **2005,** (37), 4723-4725.
137. Le Goff, A.; Artero, V.; Jousselme, B.; Tran, P. D.; Guillet, N.; Métayé, R.; Fihri, A.; Palacin, S.; Fontecave, M., From Hydrogenases to Noble Metal–Free Catalytic Nanomaterials for H₂ Production and Uptake. *Science* **2009,** *326* (5958), 1384.
138. Concepcion, J. J.; Jurss, J. W.; Brennaman, M. K.; Hoertz, P. G.; Patrocinio, A. O. T.; Murakami Iha, N. Y.; Templeton, J. L.; Meyer, T. J., Making Oxygen with Ruthenium Complexes. *Accounts of Chemical Research* **2009,** *42* (12), 1954-1965.
139. Dismukes, G. C.; Brimblecombe, R.; Felton, G. A. N.; Pryadun, R. S.; Sheats, J. E.; Spiccia, L.; Swiegers, G. F., Development of Bioinspired Mn4O4−Cubane Water Oxidation Catalysts: Lessons from Photosynthesis. *Accounts of Chemical Research* **2009,** *42* (12), 1935-1943.
140. Maeda, K.; Teramura, K.; Lu, D.; Saito, N.; Inoue, Y.; Domen, K., Noble-Metal/Cr2O3 Core/Shell Nanoparticles as a Cocatalyst for Photocatalytic Overall Water Splitting. *Angewandte Chemie International Edition* **2006,** *45* (46), 7806-7809.
141. Li, X.; Kikugawa, N.; Ye, J., Nitrogen-doped Lamellar Niobic Acid with Visible Light-responsive Photocatalytic Activity. *Advanced Materials* **2008,** *20* (20), 3816-3819.
142. Nico, C.; Monteiro, T.; Graça, M. P. F., Niobium oxides and niobates physical properties: Review and prospects. *Progress in Materials Science* **2016,** *80*, 1-37.
143. Lopes, O. F.; Mendonça, V. R. d.; Silva, F. B.; Paris, E. C.; Ribeiro, C., Niobium oxides: an overview of the synthesis of Nb2O5 and its application in heterogeneous photocatalysis. *Química nova* **2015,** *38* (1), 106-117.
144. Nowak, I.; Ziolek, M., Niobium compounds: preparation, characterization, and application in heterogeneous catalysis. *Chemical Reviews* **1999,** *99* (12), 3603-3624.
145. Ziolek, M., Niobium-containing catalysts—the state of the art. *Catalysis Today* **2003,** *78* (1), 47-64.
146. Bizeto, M. A.; Shiguihara, A. L.; Constantino, V. R. L., Layered niobate nanosheets: building blocks for advanced materials assembly. *Journal of Materials Chemistry* **2009,** *19* (17), 2512-2525.
147. Sarahan, M. C.; Carroll, E. C.; Allen, M.; Larsen, D. S.; Browning, N. D.; Osterloh, F. E., K4Nb6O17-derived photocatalysts for hydrogen evolution from water: Nanoscrolls versus nanosheets. *Journal of Solid State Chemistry* **2008,** *181* (7), 1678-1683.
148. Ebina, Y.; Sasaki, T.; Watanabe, M., Study on exfoliation of layered perovskite-type niobates. *Solid State Ionics* **2002,** *151* (1), 177-182.
149. Shiguihara, A. L.; Bizeto, M. A.; Constantino, V. R. L., Exfoliation of layered hexaniobate in tetra(n-butyl)ammonium hydroxide aqueous solution. *Colloids and Surfaces A: Physicochemical and Engineering Aspects* **2007,** *295* (1), 123-129.

150. Ravishankar, T. N.; de O. Vaz, M.; Ramakrishnappa, T.; Teixeira, S. R.; Dupont, J., Ionic liquid–assisted hydrothermal synthesis of Nb/TiO2 nanocomposites for efficient photocatalytic hydrogen production and photodecolorization of Rhodamine B under UV-visible and visible light illuminations. *Materials Today Chemistry* **2019,** *12*, 373-385.
151. Yang, M.; Kim, D.; Jha, H.; Lee, K.; Paul, J.; Schmuki, P., Nb doping of TiO2 nanotubes for an enhanced efficiency of dye-sensitized solar cells. *Chemical Communications* **2011,** *47* (7), 2032-2034.
152. Emeline, A. V.; Furubayashi, Y.; Zhang, X.; Jin, M.; Murakami, T.; Fujishima, A., Photoelectrochemical Behavior of Nb-Doped TiO2 Electrodes. *The Journal of Physical Chemistry B* **2005,** *109* (51), 24441-24444.
153. Singh, R.; Ryu, I.; Yadav, H.; Park, J.; Jo, J. W.; Yim, S.; Lee, J.-J., Non-hydrolytic sol-gel route to synthesize TiO2 nanoparticles under ambient condition for highly efficient and stable perovskite solar cells. *Solar Energy* **2019,** *185*, 307-314.
154. Huang, Q.-Z.; Wang, J.-C.; Wang, P.-P.; Yao, H.-C.; Li, Z.-J., In-situ growth of mesoporous Nb2O5 microspheres on g-C3N4 nanosheets for enhanced photocatalytic H2 evolution under visible light irradiation. *International Journal of Hydrogen Energy* **2017,** *42* (10), 6683-6694.
155. Wen, P.; Ai, L.; Liu, T.; Hu, D.; Yao, F., Hydrothermal topological synthesis and photocatalyst performance of orthorhombic Nb2O5 rectangle nanosheet crystals with dominantly exposed (010) facet. *Materials & Design* **2017,** *117*, 346-352.
156. Nunes, B. N.; Patrocinio, A. O. T.; Bahnemann, D. W., Influence of the preparation conditions on the morphology and photocatalytic performance Pt-modified hexaniobate composites. *J Phys Condens Matter* **2019,** *31* (39), 394001.
157. Chen, J.; Wang, H.; Zhang, Z.; Han, L.; Zhang, Y.; Gong, F.; Xie, K.; Xu, L.; Song, W.; Wu, S., Ultrathin HNb3O8 nanosheets with oxygen vacancies for enhanced photocatalytic oxidation of amines under visible light irradiation. *Journal of Materials Chemistry A* **2019,** *7* (10), 5493-5503.
158. Liang, S.; Wen, L.; Lin, S.; Bi, J.; Feng, P.; Fu, X.; Wu, L., Monolayer HNb3O8 for Selective Photocatalytic Oxidation of Benzylic Alcohols with Visible Light Response. *Angewandte Chemie International Edition* **2014,** *53* (11), 2951-2955.
159. Zhang, H.; Wang, Y.; Yang, D.; Li, Y.; Liu, H.; Liu, P.; Wood, B. J.; Zhao, H., Directly Hydrothermal Growth of Single Crystal Nb3O7(OH) Nanorod Film for High Performance Dye-Sensitized Solar Cells. *Advanced Materials* **2012,** *24* (12), 1598-1603.
160. Li, X.; Pan, H.; Li, W.; Zhuang, Z., Photocatalytic reduction of CO2 to methane over HNb3O8 nanobelts. *Applied Catalysis A: General* **2012,** *413-414*, 103-108.
161. Hmadeh, M.; Hoepfner, V.; Larios, E.; Liao, K.; Jia, J.; Jose-Yacaman, M.; Ozin, G. A., New Hydrogen-Evolution Heteronanostructured Photocatalysts: Pt-Nb3O7(OH) and Cu-Nb3O7(OH). *ChemSusChem* **2014,** *7* (8), 2104-2109.
162. Xia, Y.; Liang, S.; Wu, L.; Wang, X., Ultrasmall NiS decorated HNb3O8 nanosheets as highly efficient photocatalyst for H2 evolution reaction. *Catalysis Today* **2019,** *330*, 195-202.
163. Lee, S. Y.; Kang, D.; Jeong, S.; Do, H. T.; Kim, J. H., Photocatalytic Degradation of Rhodamine B Dye by TiO2 and Gold Nanoparticles Supported on a Floating Porous Polydimethylsiloxane Sponge under Ultraviolet and Visible Light Irradiation. *ACS Omega* **2020,** *5* (8), 4233-4241.
164. Joo, J. B.; Dillon, R.; Lee, I.; Yin, Y.; Bardeen, C. J.; Zaera, F., Promotion of atomic hydrogen recombination as an alternative to electron trapping for the role of metals in the photocatalytic production of H<sub>2</sub&gt. *Proceedings of the National Academy of Sciences* **2014,** *111* (22), 7942.
165. Yang, Y. Z.; Chang, C. H.; Idriss, H., Photo-catalytic production of hydrogen from ethanol over M/TiO2 catalysts (M=Pd, Pt or Rh). *Applied Catalysis B: Environmental* **2006,** *67* (3), 217-222.

166. Matsumura, M.; Saho, Y.; Tsubomura, H., Photocatalytic hydrogen production from solutions of sulfite using platinized cadmium sulfide powder. *The Journal of Physical Chemistry* **1983,** *87* (20), 3807-3808.
167. Chen, D.; Ye, J., Photocatalytic H2 evolution under visible light irradiation on AgIn5S8 photocatalyst. *Journal of Physics and Chemistry of Solids* **2007,** *68* (12), 2317-2320.
168. Reber, J. F.; Rusek, M., Photochemical hydrogen production with platinized suspensions of cadmium sulfide and cadmium zinc sulfide modified by silver sulfide. *The Journal of Physical Chemistry* **1986,** *90* (5), 824-834.
169. Kudo, A.; Tsuji, I.; Kato, H., AgInZn7S9 solid solution photocatalyst for H2 evolution from aqueous solutions under visible light irradiation. *Chemical Communications* **2002,** (17), 1958-1959.
170. Richardson, S. D.; Willson, C. S.; Rusch, K. A., Use of Rhodamine Water Tracer in the Marshland Upwelling System. *Groundwater* **2004,** *42* (5), 678-688.
171. Kornbrust, D.; Barfknecht, T., Testing of 24 food, drug, cosmetic, and fabric dyes in the in vitro and the in vivo/in vitro rat hepatocyte primary culture DNA repair assays. *Environmental Mutagenesis* **1985,** *7* (1), 101-120.
172. Nagaraja, R.; Kottam, N.; Girija, C. R.; Nagabhushana, B. M., Photocatalytic degradation of Rhodamine B dye under UV/solar light using ZnO nanopowder synthesized by solution combustion route. *Powder Technology* **2012,** *215-216*, 91-97.